Kondo Effect in Single-Walled Carbon Nanotubes

Alina Hriscu*
Zernike Institute for Advanced Materials, University of Groningen, Nijenborgh 4, 9747 AG Groningen, The Netherlands
(Dated: June 10, 2007)

In orthodox treatments of the Kondo effect the electron-electron interaction is usually neclected, because in 3D the electron system can be described as a gas of almost non-interacting particles. The situation is different in one dimension, where repulsive interactions forces the Fermi liquid to change in a Luttinger-Tomonaga liquid. The conventional Kondo effect is reviewed from a theoretical point of view. Carbon nanotubes are quantum wires that have been found to act as 1D systems. Properties of carbon nanotubes are reviewed, such as the giant Aharonov-Bohm effect in the bandgap and a Landau-level formation in magnetic fields and the absence of backward scattering. We recall the singularities of the Fermi-liquid theory in 1D, moving on to the more appropriate Tomonaga-Luttinger liquid. Furthermore, we turn on the Kondo effect in such a one-dimensional electron gas with repulsive interactions. Finally, we compare the theoretical predictions with the realm of the experimental facts.

Contents

Introduction

Why would anyone still want to study a physical phenomenon that was discovered in the 1930s, explained in the 1960s and has been subject to numerous reviews since the 1970s? Although the Kondo effect is a well known and widely studied phenomenon in condensed matter physics, it continues to capture the imagination of experimentalists and theorists alike.

The effect arises from the interactions between a single magnetic atom and the many electrons in an otherwise non-magnetic metal. The spin of the magnetic impurity interacts with the electrons in the host metal. As a result, the mathematical description of the system is a difficult many-body problem.

However, the Kondo problem is well defined, making it an attractive testing ground for the new numerical and analytical tools that have been developed to treat other many-body problems. Interest in the Kondo effect has therefore persisted because it provides clues to understanding the electronic properties of a wide variety of materials where the interactions between the electrons are particularly strong, for instance in heavy-fermion materials and high temperature superconductors.

Nonetheless, interest in the Kondo effect has recently peaked thanks to the new experimental techniques from the rapidly developing field of nanotechnology, which have given us unprecedented control over Kondo systems [1].

Metallic carbon nanotubes(CNT) are quantum wires that have been found to act as one-dimensional quantum dots, Luttinger liquids, proximity-induced superconductors and ballistic and diffusive 1D metals. Therefore, they provide a very rich field of research. Kondo effect has been reported in CNT, proving the universality of the Kondo effect.

I. CONVENTIONAL KONDO EFFECT

The Kondo effect represents a rare(if not unique) example of phenomenon named after the theorist who first explained it [2]. The anomalous *resistance minimum*, as the Kondo effect was known prior to 1964, was discovered in 1930s by de Haas et al. [3] yet it took 34 years for a satisfactory theoretical explanation to appear.

The electrical resistance of a pure metal usually drops

*Electronic address: A.M.Hriscu@student.rug.nl

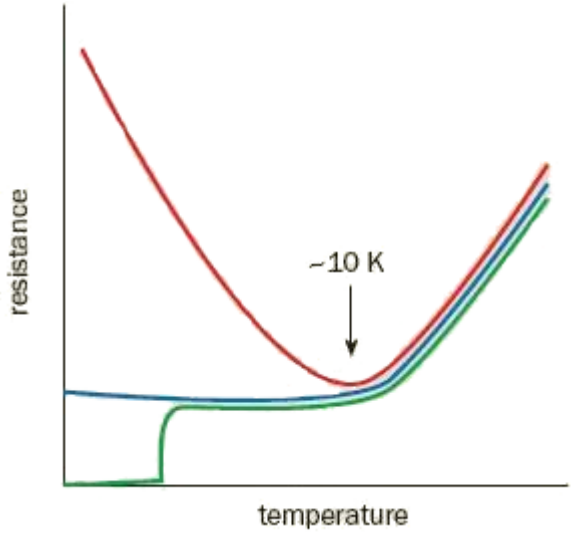

FIG. 1: As the temperature of a metal is lowered, its resistance decreases until it saturates at some residual value(blue). Some metals become superconducting at a critical temperature(green). However, in metals that contain a small fraction of magnetic impurities, such as cobalt-copper systems, the resistance increases at low temperatures due to the Kondo effect(red). Figure from Kouwenhoven and Glazman [1].

as its temperature is lowered because electrons can travel through a metallic crystal more easily when the vibrations of the atoms are small. However, the resistance saturates as the temperature is lowered below about 10 K due to static defects in the material (figure 1).

Some metals, for example lead, niobium and aluminium can suddenly lose their resistance to the electrical current and become superconducting. This phase transition from a conducting to a superconducting state occurs at the *critical temperature*, below which the electrons behave as a single entity. Indeed, superconductivity is a prime example of a many body phenomenon.

Other metals, like copper and gold, remain conducting and have a constant finite resistance, even at the lowest accessible temperatures. The value of the low-temperature resistance depends on the number of defects in the material. Adding defects increases the value of this "saturation resistance" but the character of the temperature dependence remains the same.

However, this behaviour changes dramatically when magnetic atoms, such as cobalt, iron or rare earths such as cerium are added. Rather than saturating, the electrical resistance increases as the temperature is lowered further. Although this behaviour does not involve a phase transition, the so-called Kondo temperature - roughly speaking the temperature at which the resistance starts to increase again - completely determines the low temperature electronic properties of the material, as we shall see further in this section.

Electrical resistance is related to the amount of back scattering from defects, which hinders the motion of the electrons through the crystal. Theorists can readily calculate the probability with which an electron will be scattered when the defect is small. However, for larger defects, the calculation can only be performed using perturbation theory, in which the answer is written as a series of smaller and smaller terms. In 1964 Kondo made a startling discovery when considering the scattering from a magnetic ion that interacts with the spins of the conducting electrons. He found that the second term in the calculation could be much larger than the first. The upshot of this result is that the resistance of a metal increases logarithmically as the temperature is lowered.

Kondo's theory correctly describes the observed upturn of the resistance at low temperature. However, it also makes the unphysical prediction that the resistance will be infinite at even lower temperatures. It turns out that Kondo's result is correct only above a certain temperature, which became known as Kondo temperature, T_K.

The theoretical background for understanding the physics below T_K emerged in the late 1960s from Phil Anderson's idea of "scaling" in the Kondo problem. Scaling assumes that the low-temperature properties of a real system are adequately represented by a coarse-grained model. As the temperature is further lowered, the model becomes coarser and the number of degrees of freedom it contains is reduced. This approach can be used to predict the properties of a real system close to absolute zero.

Later, in 1974, K. Wilson devised the method known as "numerical renormalization" that overcame the shortcomings of conventional perturbation theory, and confirmed the scaling hypothesis. His work proved that at temperatures below T_K, the magnetic moment of the impurity is screened entirely by the spins of the electrons in the metal.

We discuss the explanation provided by Kondo in the next subsection. The renormalization problem is not included here.

A. Kondo's explanation of the resistance minimum

The resistivity of a metal at temperatures much lower than Debye temperature, the resistivity should be given by an expression of the form [4]

$$\rho(T) = \rho_0 + AT^5. \tag{1.1}$$

Here the T^5 behaviour comes from electron-phonon scattering, while the impurities in the metal give rise to the constant term ρ_0.

When small amounts of iron, chromium, manganese, molybdenum, rhenium or osmium are added to copper, silver, gold, magnesium or zinc, for example, the resistivity behaviour changes, exhibiting a minimum. The effect arises only when the defects are magnetic, in other words, when the total spin of all the electrons in the impurity

atom is non-zero. These electrons coexist with the mobile electrons in the host metal, which behave like a Fermi sea. The temperature at which the resistivity reaches the minimum value is quite low, and does not appear to be related to the Fermi temperature $T_F = \varepsilon_F/k$ or to the Debye temperature Θ, but seems to vary with the impurity concentration n_i roughly as $n_i^{1/5}$.

The magnetic impurity contribution to the resistivity was cast in the form of an empirical law

$$\delta\rho(T) \propto n_i \ln(\varepsilon_F/T). \tag{1.2}$$

Since the contribution to the resistivity from the electron-phonon scattering decreases with the decrease of T (see eq. 1.1), eq. 1.2 leads to a minimum of the resistivity at a certain temperature. The relation $\delta\rho(T) \propto n_i$ has been verified down to the lowest attainable impurity concentrations, thereby establishing that the phenomenon is a single impurity effect rather than arising from the interaction between the impurities. These observations [5] led Kondo to consider the simplest possible model describing the exchange interaction of a magnetic impurity with the conduction electrons in the host metal,

$$H_{\mathrm{K}} = H_0 + J(\mathbf{s}\cdot\mathbf{S}), \tag{1.3}$$

where $H_0 = \sum_{k\sigma} \xi_k c^\dagger_{k\sigma} c_{k\sigma}$ describes the electron gas, $\mathbf{s} = \frac{1}{2}\sum_{kk'\sigma\sigma'} c^\dagger_{k\sigma}\hat{\tau}_{\sigma\sigma'} c_{k'\sigma'}$ is the spin density of the conduction electrons at the impurity site (with $\hat{\tau} = (\hat{\tau}^x, \hat{\tau}^y, \hat{\tau}^z)$ being the Pauli matrices), and $\mathbf{S}$ is a spin-1/2 operator representing the magnetic impurity. The phenomenological Kondo model 1.3 (a.k.a the $s-d$ model) was introduced into the literature at least as early as in 1946 [6]; its validity was later established [7] by deriving it from the microscopic Anderson impurity model [8]. One can define the spin raising and lowering operators s^+, s^-, S^+, S^- for the Bloch states in the Fermi sea and localised electrons of the impurity, respectively. With these new operators the factor $\mathbf{s}\cdot\mathbf{S}$ takes the form [4]

$$\mathbf{s}\cdot\mathbf{S} = \frac{1}{2}\left(s^+S^- + s^-S^+\right) + s^zS^z$$

In the notation of the second quantization for the Bloch states we can write the perturbation as

$$H_1 = \sum_{k,k',\sigma,\sigma'} V_{kk'}/(\hbar^2) c^\dagger_{k'\sigma'} c_{k\sigma} \langle\sigma'|\mathbf{s}\cdot\mathbf{S}|\sigma\rangle.$$

In this expression $c^\dagger, c$ are the electron creation and the annihilation operators respectively, σ and σ' refer to spin states of the Bloch electrons. $V_{kk'}$ is the matrix element of interaction between Bloch conduction-band states of the spatial part $V(\mathbf{r})$ of the perturbing spin-dependent interaction due to an impurity at the origin,

$$V_{kk'} = \int \mathrm{dr}\ \psi^*_k V(\mathbf{r}) \psi_{k'}.$$

Because $V(\mathbf{r})$ extends over only about one unit cell, while the wavefunction extends over the whole crystal, this quantity is of the order N^{-1}, with N the number of unit cells in the crystal. The only non-vanishing matrix element of s^+ is $\langle\uparrow|s^+|\downarrow\rangle = \hbar$, and for s^- only $\langle\downarrow|s^-|\uparrow\rangle = \hbar$ survives, while s^z has elements $\langle\uparrow|s^z|\uparrow\rangle = \hbar/2$ and $\langle\downarrow|s^z|\downarrow\rangle = -\hbar/2$. Thus

$$H_1 = \frac{1}{2\hbar}\sum_{k,k'} V_{kk'}\left[c^\dagger_{k'\uparrow}c_{k\downarrow}S^- + c^\dagger_{k'\downarrow}c_{k\uparrow}S^+ + (c^\dagger_{k'\uparrow}c_{k\uparrow} - c^\dagger_{k'\downarrow}c_{k\downarrow}S^-)S^z\right]. \tag{1.4}$$

Diagrams illustrating the type of scattering caused by each of these terms would then be of the form shown in figure 2. The scattering probability is proportional to the elements of the the *transition matrix* (T-matrix) for this perturbation. In the Born approximation the T-matrix is replaced by H_1 itself, and then the scattering probability is found from terms with precisely two annihilation operators and two creation operators, and turns out to be composed of terms of the form

$$Q(k,k')N_{k\downarrow}(1-N_{k'\uparrow})$$

corresponding to the process depicted in figure 2 (a) and other terms corresponding to the other processes. Here $Q(k,k')$ represents the probability that in unit time an electron is scattered between the Bloch state with wavevector k' and the perturbed state with k. The scattering is elastic, since we are not assuming the energy of the impurity depend on its spin direction after the Bloch electron has scattered and departed. The various occupation numbers N_k can be averaged to give the f_k that enter the Boltzmann equation.

The interesting effects, as already mentioned, occur when considering the second-order terms in the T-matrix. Let us for simplicity look at those processes in which the

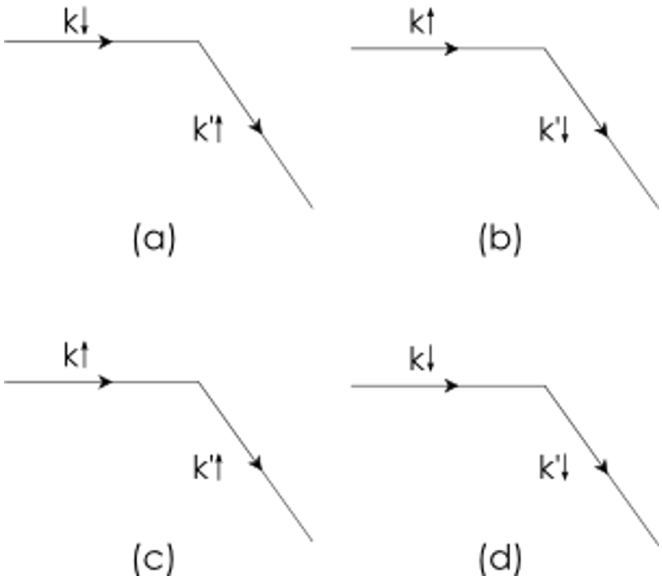

FIG. 2: In the Born approximation a magnetic impurity can scatter an electron in these four different ways. Figure adapted from Taylor [4].

net result is that an electron in the state $\mathbf{k}\uparrow$ is scattered into the state $\mathbf{k}'\downarrow$. While in the first order only the process shown in figure 2(c) contributes to this, there are other possibilities in the second order. We recall [4] that

$$T = H_1 + H_1\frac{1}{\varepsilon - H_0}T \approx H_1 + H_1\frac{1}{\varepsilon - H_0}H_1$$

to the second order. Of the sixteen types of second-order term that we find when we substitute expression 1.4 into this, we examine only those two involving products of S^+ with S^-. These are sums of the form

$$\frac{1}{(2\hbar)^2}\sum_{k_1k_2k_3k_4} V_{k_1k_2}V_{k_3k_4}c^\dagger_{k_1\uparrow}c_{k_2\downarrow}S^-\frac{1}{\varepsilon - H_0}c^\dagger_{k_3\downarrow}c_{k_4\uparrow}S^+ \tag{1.5}$$

and

$$\frac{1}{(2\hbar)^2}\sum_{k_1k_2k_3k_4} V_{k_1k_2}V_{k_3k_4}c^\dagger_{k_3\downarrow}c_{k_4\uparrow}S^+\frac{1}{\varepsilon - H_0}c^\dagger_{k_1\uparrow}c_{k_2\downarrow}S^-. \tag{1.6}$$

For these to have the net effect of scattering $\mathbf{k}\uparrow$ into $\mathbf{k}'\uparrow$ we must always have $\mathbf{k_2} = \mathbf{k_3}$, $\mathbf{k_4} = \mathbf{k}$ and $\mathbf{k_1} = \mathbf{k}'$. In terms of diagrams we can picture these processes as in figure 3(a).

The diagram (a) represents expression 1.5, in which an electron is first scattered from $\mathbf{k}\uparrow$ to the virtual state $\mathbf{k_2}\downarrow$, and then finally to the state $\mathbf{k}'\uparrow$. In diagram (b), however, the first thing that happens is the creation of an electron-hole pair. That is, an electron already in state $\mathbf{k_2}\downarrow$ is scattered into $\mathbf{k}'\uparrow$. The incoming electron in the state $\mathbf{k}\uparrow$ then drops down into this vacancy in a process that we can depict as the annihilation of an electron-hole

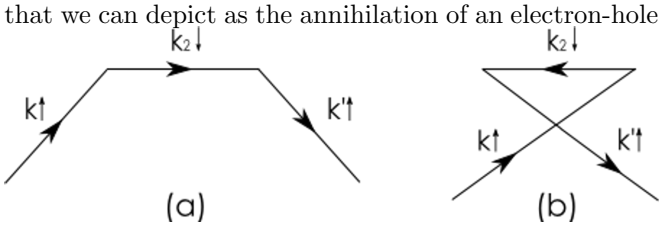

FIG. 3: These two second-order processes both contribute to the scattering amplitude for a conduction electron. Because of the change of spin, the occupancy N_{k_2} of the intermediate state does not cancel from the total scattering amplitude. Figure adapted from Taylor [4].

pair. The energy of the intermediate state differs from that of the initial state by $\varepsilon_{k'} - \varepsilon_{k_2}$, which is just the negative of the energy difference $\varepsilon_{k_2} - \varepsilon_k$ of the process of figure 3(a). We can thus add the contributions of the expressions 1.5 and 1.6 and use the anticommutation relations of the creation and annihilation operators c's and $c^\dagger$'s to find

$$\frac{1}{(2\hbar)^2}\sum_{k_2} V_{k'k_2}V_{k_2k}c^\dagger_{k'\uparrow}c_{k\uparrow}\frac{1}{\varepsilon_k - \varepsilon_0}\left[(1-N_{k_2\downarrow})S^-S^+ + N_{k_2\downarrow}S^+S^-\right]. \tag{1.7}$$

If S^+ and S^- were not operators but simply numbers they would commute, and the terms in N_{k_2} would cancel. We would then be back in the situation of having the type of scattering that leads to a temperature-independent resistivity. But using the commutation relation

$$S^-S^+ - S^+S^- = -2\hbar S_z,$$

one gets a contribution to the scattering matrix that is proportional to

$$c^\dagger_{k'\uparrow}c_{k\uparrow}S_z\sum_{k_2} V_{k'k_2}V_{k_2k}\frac{\langle N_{k_2\downarrow}\rangle}{\varepsilon_k - \varepsilon_0}. \tag{1.8}$$

The presence of the term in N_{k_2} has the consequence that the scattering probability becomes strongly temperature-dependent. Denoting the sum after k_2 in expression 1.8 by $g(\mathbf{k}', \mathbf{k})$ when we form $\mid T_{\mathbf{k}\mathbf{k}'} \mid^2$ we shall find contribu-

tions of the form

$$P_K(\mathbf{k}\uparrow,\mathbf{k}'\uparrow) \propto \langle N_{k\uparrow}(1-N_{k'\uparrow})\rangle g(\mathbf{k}',\mathbf{k}).$$

The subscript K refers to the contributions responsible for the Kondo effect. Because the thermal average of the expectation value of $N_{k_2\downarrow}$ is given by the Fermi-Dirac function, we see that $g(\mathbf{k}',\mathbf{k})$ depends on the temperature.

The total probability $P(\mathbf{k}\uparrow,\mathbf{k}'\uparrow)$ of a scattering event occurring in which the net effect is that an electron is transferred from $\mathbf{k}\uparrow$ to $\mathbf{k}'\uparrow$ can be written as

$$P(\mathbf{k}\uparrow,\mathbf{k}'\uparrow) = f_{k\uparrow}(1-f_{k'\uparrow})Q(\mathbf{k}',\mathbf{k}).$$

Here $Q(\mathbf{k}',\mathbf{k})$ is composed of two parts. One is independent of the temperature and is due to first-order precesses plus those contributions from higher-order processes that do not involve the occupation numbers of the intermediate states. The second part contains contributions from the occupation numbers of the intermediate states, and in second order has the temperature dependence of $g(\mathbf{k}',\mathbf{k})$. The qualitative nature of this temperature dependence may be seen by making a few approximations. We first assume that the matrix elements $V_{k'k_2}$ and V_{k_2k} vary slowly over the range of energies over which we have to integrate $\mathbf{k}_2$ so that we can replace each of them by a constant V_0. We can then change from a sum over $\mathbf{k}_2$ to an integration over energies ε_2 by introducing the density of states $D(\varepsilon)$, and then approximate this by its value when ε_{k_2} is equal to the chemical potential μ. We specialize to the value of $g(\mathbf{k}',\mathbf{k})$ when ε_k is also equal to μ to find

$$g(\mathbf{k}',\mathbf{k}) \approx V_0^2 D(\mu)\int_{-W}^{W} d\hat{\varepsilon}\frac{f(\hat{\varepsilon})}{\hat{\varepsilon}},$$

where W is an energy characteristic of the width of the band. After inserting the form of the Fermi-Dirac function f and defining $x \equiv \hat{\varepsilon}/2k_BT$ we have

$$g(\mathbf{k}',\mathbf{k}) \approx -V_0^2 D(\mu)\int_0^{W/2k_BT} dx\frac{\tanh x}{x}.$$

The integral is easily calculated. It is the same integral as the found for the critical temperature of a BCS superconductor, and so we find the result

$$g(\mathbf{k}',\mathbf{k}) \approx -V_0^2 D(\mu)\ln(1.14W/k_BT).$$

The low-temperature resistivity then takes the form

$$\rho(T) = \rho_0 + \rho_1(\frac{T}{\Theta})^5 - \rho_2\ln(\frac{k_BT}{W}). \qquad (1.9)$$

The resistance has its minimum when the derivative $d\rho/dT$ vanishes. Thus,

$$5\rho_1\frac{T_{min}^4}{\Theta^5} - \frac{\rho_2}{T_{min}} = 0$$

and

$$T_{min}^5 = \frac{\rho_2\Theta^5}{5\rho_1}.$$

For low impurities concentrations, the scattering events on different impurities are independent and their contributions add incoherently. The sum over scattering events on all impurities is then proportional to the concentration n_i of impurities, so we have shown that

$$T_{min} \propto n_i^{1/5}.$$

The fact that equation 1.9 erroneously predicts an infinite resistance as T approaches zero is a consequence of the inadequacy if considering only second-order terms in the T-matrix, and of our implicit high-temperature assumption that the energy of the local spins is independent of its orientation. At lower temperatures the local spins form bound collective states with the conduction-band electrons. In order to flip the local spin , this binding must be broken by thermal energy of excited conduction electrons. As the temperature is reduced this becomes more and more unlikely, and the local spin becomes "frozen out". In fact, the singularity signals this formation of a bound state. The problem of dealing with these divergencies became known as the *Kondo problem*, and its resolution came later with the advent of the powerful Renormalization Group ideas [9, 10].

The definition of the Kondo temperature T_K is given by

$$k_BT_K \equiv W\exp\left(-\frac{1}{2D\mid J\mid}\right). \qquad (1.10)$$

In this expression J is the antiferromagnetic coupling constant between electrons above the Fermi sea, or of the holes below it with the local spins. We again notice an analogy with the BCS theory of superconductivity, in which one finds a similar expression for the critical temperature T_c. This is not an accident. Both T_K and T_c define temperatures below which perturbation theory fails. In the BCS case, T_c signals the onset of the formation of bound Cooper pairs and a new ground state with an energy gap. The Kondo effect is a little more subtle. Here T_K defines a temperature at which the energy contributions from second-order perturbation theory become important. This happens when the local spin on a single impurity starts to become frozen out at an energy set by the Kondo coupling J and the density of states at the Fermi energy.

Kondo's discovery solved one of the longest standing puzzles in the history of condenses matter physics.

In the low temperature limit (which is not going to be discussed here in detail- see [4] for detailed discussion) the internal dynamics of the local spins interacting with the sea of conduction electrons become important. The net effect of this interaction is very much like a resonant state appearing at temperatures $\sim T_K$. In fact, Wilkins [11]

has noted that the Kondo effect is very well described by a density-of-states expression that adds a resonant state at the Fermi energy for each impurity with a local moment. He writes an expression as

$$D_K(\varepsilon) = D(\varepsilon) + \frac{c}{\pi}\frac{\gamma}{(\varepsilon - \varepsilon_F)^2 + \gamma^2} = D(\varepsilon) + \delta D(\varepsilon) \tag{1.11}$$

where $\gamma = 1.6 k_B T_K$. This expression adds a Lorentzian peak of weight unity at the Fermi energy for each impurity atom with a local moment. From this expression one can calculate, for example, the change in specific heat and the change in electrical resistance. All the many-body physics has then resulted in a simple change in the density of states at the Fermi surface consisting of the addition of a resonant state for each impurity. At high temperatures, the sharp resonances are unimportant in the presence of thermal smearing at the Fermi surface. However, as the temperature is decreased, the sharp resonances become more important in the scattering of the conduction electrons. At still lower temperatures, there is insufficient energy to flip the local spins, which become frozen in fixed orientations.

Briefly, at low temperature the electrons of the host tend to screen the local spin of the magnetic impurity, resulting in a change of the local DOS at E_F around the site of the magnetic impurity, i.e., the emergence of a Kondo resonance.

The Kondo resonance is unusual. Energy eigenstates usually correspond to waves for which an integer number of half wavelengths fits precisely inside a quantum box, or around the orbital of an atom. In contrast, the Kondo state is generated by exchange processes between a localized electron and free-electron states.Since many electrons need to be involved, the Kondo effect is a many-body phenomenon. It is important to note that that the Kondo state is always on resonance since it is fixed to the Fermi energy. Even though the system may start with an energy, ε_0 , that is very far away from the Fermi energy, the Kondo effect alters the energy of the system so that it is always on resonance.The only requirement for the effect to occur is that the metal is cooled to sufficiently low temperatures below the Kondo temperature T_K.

II. CARBON NANOTUBES AND THEIR PROPERTIES

Carbon nanotubes (CNTs) are allotropes of carbon. A single wall carbon nanotube is a one-atom thick sheet of graphene rolled up into a seamless cylinder with diameter of the order of a nanometer. This results in a nanostructure where the length-to-diameter ratio exceeds 10,000.

S. Iijima brought carbon nanotubes into the awareness of the scientific community in 1991 [12]. Ever since, carbon nanotubes have aroused great excitement. What is so special about them? The answer lies in their unique physical properties, which span a wide range-from structural to electronic. For example, nanotubes have a light

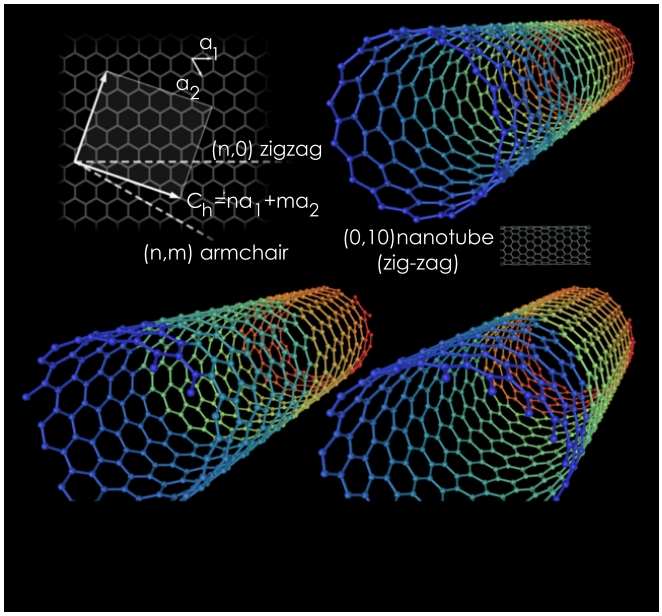

FIG. 4: 3D model of three types of single-walled carbon nanotubes. Figure from wikipedia.org.

weight and a record-high elastic modulus, and they are predicted to be by far the strongest fibers that can be made. Their high strength is accompanied by their ability to buckle in a reversible manner: when a tube is bent, it does not directly fracture like most materials but buckles like a drinking straw. When the bending strain is released, the tube straightens out again. Such remarkable mechanical properties are relevant to a broad range of potential applications. Similarly, the capillary properties of nanotubes hold promise in applications such as catalysis and energy storage. Then there are the exceptional electrical properties of nanotubes. As described below, nanotubes can be semiconductors or metals, and they display exciting quantum wire properties.

A. Energy bands and Aharonov-Bohm effect

Single-walled nanotubes (SWNT) are a very important variety of carbon nanotubes because they exhibit important electric properties that are not shared by the multi-walled carbon nanotube (MWNT) variants. Experiments have revealed a great deal about their electronic properties. Most single-walled nanotubes (SWNT) have a diameter of close to 1 nanometer, with a tube length that can be many thousands of times longer. The structure of a SWNT can be conceptualized by wrapping a one-atom-thick layer of graphene into a seamless cylinder. The conductive properties of nanotubes depend drastically on both the diameter and the chirality of the hexagonal carbon lattice along the tube. A slight change in the winding of hexagons along the tube can transform the tube from a metal into a large-gap semiconductor. It turns

out that about two-thirds of tubes are semiconducting and one-third are metallic. The way the graphene sheet is wrapped is represented by a pair of indices (n,m) called the chiral vector. The integers n and m denote the number of unit vectors along two directions in the honeycomb crystal lattice of graphene. If m=0, the nanotubes are called "zigzag". If n=m, the nanotubes are called "armchair". Otherwise, they are called "chiral" (see figure 4). STM measurements have verified that they are indeed 1D semiconductors or conductors, depending on their chirality[13].

The condition of whether a CNT is metallic or semiconducting can be obtained based on the band structure of a 2D graphite sheet and periodic boundary conditions along the circumference direction. This result was first predicted by means of a tight-binding model ignoring the effect of the tube curvature [14]. These properties can be well reproduced in a $\mathbf{k}\cdot\mathbf{p}$ method or an effective-mass approximation. In fact, the effective-mass scheme has been used successfully in the study of wide varieties of electronic properties of CNT. Some examples are magnetic properties [15] including the Aharonov-Bohm effect on the bandgap [15], optical absorption spectra [16], exciton effects [17], lattice instabilities in the absence [18] and presence of a magnetic field [19], and magnetic properties of ensembles of nanotubes [19].

Graphene is a semimetal with valence and conduction bands degenerate at only six corners ($\mathbf{K}_B$) of the hexagonal first Brillouin zone. The Fermi surface of the graphene sheet is thus reduced to these six points (see figure 6).

Figure 5 shows the lattice structure and the first Brillouin zone of graphene together with the coordinate systems of a nanotube. The unit cell of the graphene has an area $\sqrt{3}a^2/2$ and contains two carbon atoms (denoted as A and B). A nanotube is specified by a chiral vector $L = n_a a + n_b b$ with integer n_a and n_b and basis vectors a and b ($|\mathbf{a}| = |\mathbf{b}| = a$ =2.46 Å). In the coordinate system fixed onto a graphite sheet, we have $\mathbf{a} = (a, 0)$ and $\mathbf{b} = (-a/2, \sqrt{3}a/2)$. For convenience we introduce another coordinate system where the x direction is along the circumference L and the y direction is along the axis of CNT. The direction of L is denoted by the chiral angle η.

A graphite sheet is a zero-gap semiconductor in the sense that the conduction and valence bands consisting of π states cross at K and K' points of the Brillouin zone, whose wave vectors are given by $\mathbf{K} = (2\pi/a)(1/3, 1/\sqrt{3})$ and $\mathbf{K'} = (2\pi/a)(2/3,0)$, as shown in figure 7 [21]. The K and K' points are not equivalent because they are not connected by reciprocal lattice vectors.

Electronic states near a K point of graphene are described by the $\mathbf{k}\cdot\mathbf{p}$ equation [15]:

$$\gamma(\tau_x\hat{k}_x + \tau_y\hat{k}_y)\mathbf{F}_K(r) = \gamma(\tau\cdot\hat{k})F^K(r) = \varepsilon F^K(r) \quad (2.1)$$

where γ is the band parameter, $\hat{k} = (\hat{k}_x, \hat{k}_y)$ is a wave-vector operator, ε is the energy, and τ_x,τ_y and τ_z are the

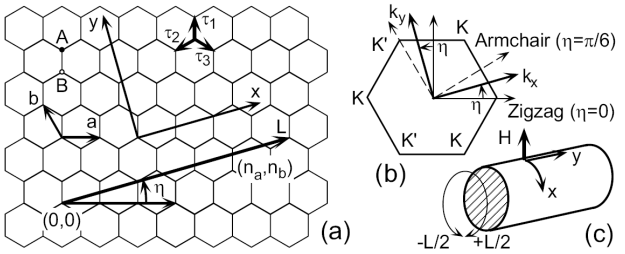

FIG. 5: (a) Lattice structure of two-dimensional graphite sheet. η is the chiral angle. The coordinates are chosen in such a way that x is along the circumference of a nanotube and y is along the axis. (b) The first Brillouin zone and K and K' points. (c) The coordinates for a nanotube. Figure from [20].

Pauli spin matrices. In the above equations, the envelope functions are written as

$$F^K(r) = \begin{pmatrix} F_A^K(r) \\ F_B^K(r) \end{pmatrix}.$$

For nanotubes with a sufficiently large diameter, their electronic states near the Fermi level can be obtained by imposing the periodic boundary condition in the circumference direction, $\Psi(r + L) = \Psi(r)$. The Bloch functions at a K point change their phase by $\exp(\imath\mathbf{K}\cdot\mathbf{L}) = \exp(2\pi\imath\nu/3)$, where ν is an integer defined by $n_a + n_b = 3M + \nu$ with integer M and can take 0 and 1. Because $\Psi(r)$ is written as a product of the Bloch function and the envelope function, this phase change should be cancelled by that of the envelope functions and the boundary conditions for the envelope functions are given by

$$F^K(r + L) = F^K(r)\exp\left(-\frac{2\pi\imath\nu}{3}\right). \quad (2.2)$$

Energy levels in CNT for the K point are obtained by putting $k_x = \kappa_\nu(n)$ with

$$\kappa_\nu(n) = \frac{2\pi}{L}\left(n - \frac{\nu}{3}\right) \quad (2.3)$$

and $k_y = k$ in the above $\mathbf{k}\cdot\mathbf{p}$ equation [15] as

$$\varepsilon_\nu^{(\pm)}(n, k) = \pm\gamma\sqrt{\kappa_\nu(n)^2 + k^2} \quad (2.4)$$

where $L = |L|, n$ is an integer, and the upper (+) and lower (-) signs represent the conduction and valence bands, respectively. Those for the K' point are obtained by replacing ν by $-\nu$ in the above equations. This shows that CNT becomes metallic for $\nu = 0$ and semiconducting with gap $E_g = 4\pi\gamma/3L$ for $\nu = \pm 1$. Figure 8 compares this gap to that obtained in a tight-binding model.

In the presence of a magnetic field, the wave-vector operators become $\hat{k} = -\imath\nabla + (e\mathbf{A}/c\hbar)$, where $A = (A_x, A_y)$ is the vector potential. When the field is parallel to the

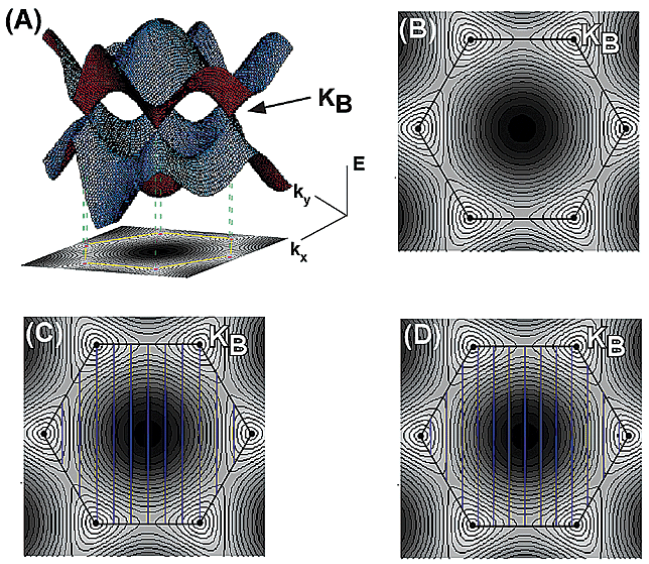

FIG. 6: (A) Three-dimensional plot of the π and π^* graphene energy bands and (B) a 2D projection. (C) Allowed 1D wavevectors for a metallic (9,0) SWNT. (D) Allowed 1D wavevectors for a semiconducting (10,0) tube. The black hexagons define the first Brillouin zone of a graphene sheet, and the black dots in the corners are the KB points. Blue lines represent allowed wavevectors, k, within the first Brillouin zone. Figure from [22].

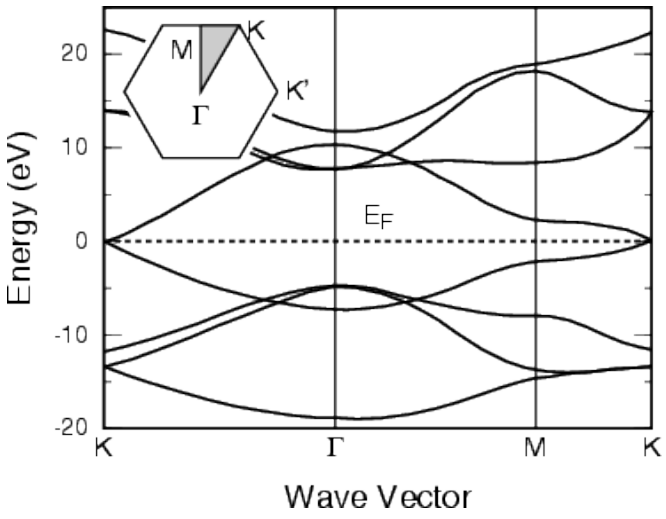

FIG. 7: Energy gap versus magnetic flux passing through the tube cross section for metallic ($\nu = 0$) and semiconducting ($\nu = \pm 1$) CNT. Figure from [20].

axis, i.e., in the presence of a magnetic flux ϕ passing through the cross section, this leads to the change in the boundary condition $\Psi(r + L) = \Psi(r) \exp(2\pi\imath\varphi)$ with $\varphi = \phi/\phi_0$, where $\phi_0 = ch/e$ is the magnetic flux quantum. Consequently, $\kappa_\nu(n)$ is replaced by $\kappa_{\nu\varphi}(n)$ with

$$\kappa_{\nu\varphi}(n) = \frac{2\pi}{L}\left(n + \varphi - \frac{\nu}{3}\right). \qquad (2.5)$$

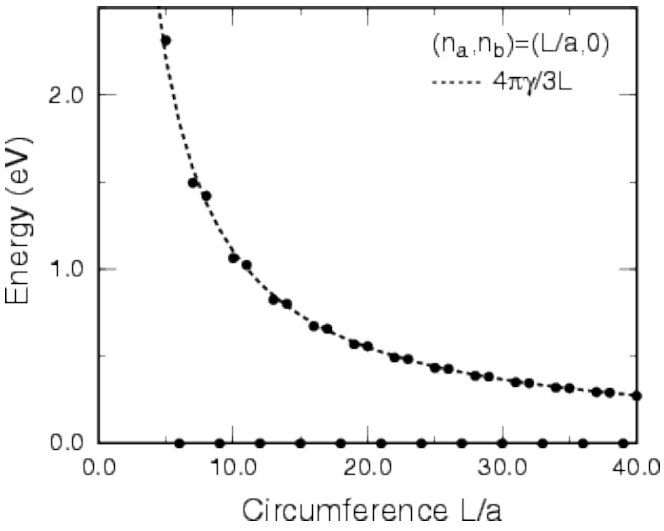

FIG. 8: The bandgap of a zigzag nanotube as a function of the circumference L/a. The dots represent tight-binding results and the dotted line the result of the lowest-order $\mathbf{k}\cdot\mathbf{p}$ scheme. Figure from [20].

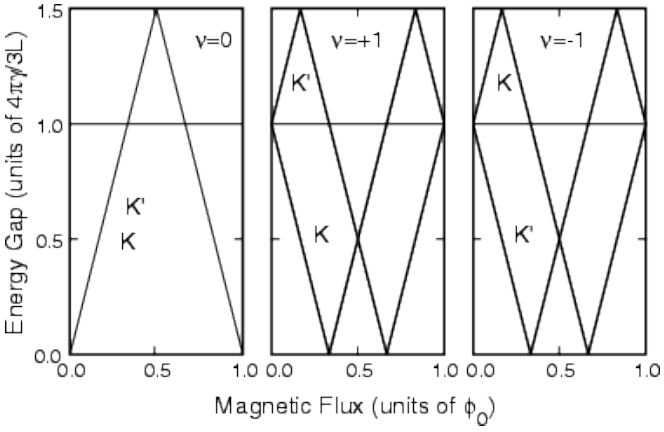

FIG. 9: Energy gap versus magnetic flux passing through the tube cross section for metallic ($\nu = 0$) and semiconducting ($\nu = \pm 1$) CN. After [15]

.

The corresponding result for the K' point is again obtained by the replacement $\nu \to -\nu$. The bandgap exhibits an oscillation between 0 and $2\pi\gamma/L$ with period ϕ_0 as shown in figure 9. This giant Aharonov-Bohm (AB) effect on the bandgap is a unique property of CNTs. The AB effect appears also in a tunnelling conductance across a finite-length CNT [23].

In the presence of a magnetic field H perpendicular to the tube axis, we can use the gauge

$$\mathbf{A} = \left(0, \frac{LH}{2\pi}\sin\frac{2\pi x}{L}\right) \qquad (2.6)$$

and the effective field for electrons in a CNT is given by the component perpendicular to the surface, i.e., $H(x) = H\cos(2\pi x/L)$. The parameter characterizing its strength

is given by $\alpha = (L/2\pi l)^2$, where $l = \sqrt{c\hbar/eH}$ is the magnetic length or the radius of the smallest cyclotron orbit. In the case $(L/2\pi l)^2 \ll 1$, the field can be regarded as a small perturbation, while in the case $(L/2\pi l)^2 \gg 1$, Landau levels are formed on the cylinder surface. An interesting feature of equation 2.1 lies in the fact that Landau levels are formed at energy $\varepsilon = 0$ independent of the field strength. This anomaly has long been known as the origin of a large diamagnetism of graphite [24],[25].

Consider a metallic nanotube for example. The energy levels and wavefunctions are analytically obtained for $\varepsilon \sim 0$ in this case [26]. The results are

$$F_{sk}^{K} = \frac{1}{\sqrt{2A}} \begin{pmatrix} -\imath s(k/|k|)F_{-}(x) \\ F_{+}(x) \end{pmatrix} \exp(\imath k y)$$

$$F_{sk}^{K'} = \frac{1}{\sqrt{2A}} \begin{pmatrix} +\imath s(k/|k|)F_{+}(x) \\ F_{-}(x) \end{pmatrix} \exp(\imath k y) \tag{2.7}$$

with

$$F_{\pm}(x) = \frac{1}{\sqrt{LI_0(2\alpha)}} \exp\left(\pm\alpha \cos\frac{2\pi x}{L}\right) \tag{2.8}$$

where A is the length of the nanotube, $s = +1$ and -1 for the conduction and valence band, respectively, and $I_0(z)$ is the modified Bessel function of the first kind defined as

$$I_0(z) = \int_0^{\pi} \frac{\mathrm{d}\theta}{\pi} \exp(z\cos\theta). \tag{2.9}$$

In high magnetic fields ($\alpha \gg 1$), F_{-} is localized around $x = \pm L/2$, i.e., at the bottom side of the cylinder and F_{+} is localized around the top side $x = 0$. The corresponding eigenenergies are given by

$$\varepsilon_s(k) = \frac{s\gamma|k|}{I_0(2\alpha)} \tag{2.10}$$

which gives the group velocity

$$v = \frac{\gamma}{\hbar I_0(2\alpha)} \tag{2.11}$$

and the density of states

$$D(0) = \frac{I_0(2\alpha)}{\pi\gamma} \tag{2.12}$$

at $\varepsilon = 0$. We should note that

$$I_0(2\alpha) \approx \begin{cases} 1 + \alpha^2 + \cdots & (\alpha \ll 1) \\ e^{2\alpha}/\sqrt{4\pi\alpha} & (\alpha \gg 1) \end{cases}$$

This means that the group velocity for states at $\varepsilon = 0$ decreases and consequently the density of states increases exponentially with the increase of the magnetic field in the high-field regime.

Figure 10 gives some examples of energy bands of a metallic CN in perpendicular magnetic fields, which clearly show the formation of flat Landau levels at the Fermi level in high fields. It is worth mentioning that there is no difference in the spectra between metallic and semiconducting CNs and in the presence and absence of an AB flux for $(L/2\pi l)^2 \gg 1$, because the wave function is localized in the circumference direction and the boundary condition becomes irrelevant.

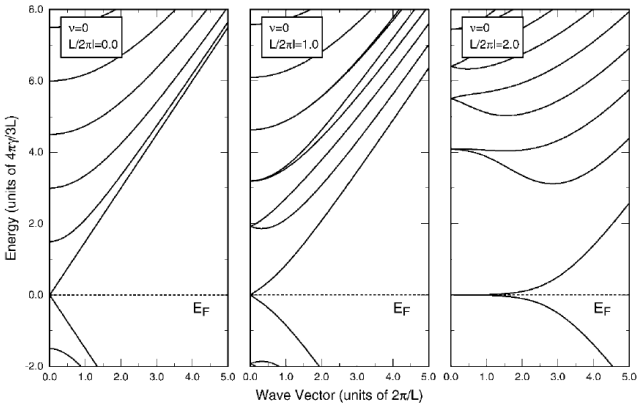

FIG. 10: Some examples of calculated energy bands of a metallic CN in magnetic fields perpendicular to the axis. After [20]

.

B. Absence of backward scattering

In the presence of impurities, electronic states in the vicinity of K and K' points can be mixed with each other. Therefore, we should use a 4×4 Schrödinger equation

$$H\mathbf{F} = \varepsilon\mathbf{F} \tag{2.13}$$

with

$$\mathbf{F} = \begin{pmatrix} \mathbf{F}^{K} \\ \mathbf{F}^{K'} \end{pmatrix} \qquad \mathbf{F}^{K'} = \begin{pmatrix} F_A^{K'} \\ F_B^{K'} \end{pmatrix} \tag{2.14}$$

and

$$H = H_0 + V. \tag{2.15}$$

The unperturbed Hamiltonian is given by

$$H_0 = \gamma \begin{pmatrix} 0 & \hat{k}_x - \imath\hat{k}_y & 0 & 0 \\ \hat{k}_x + \imath\hat{k}_y & 0 & 0 & 0 \\ 0 & 0 & 0 & \hat{k}_x + \imath\hat{k}_y \\ 0 & 0 & \hat{k}_x - \imath\hat{k} & 0. \end{pmatrix} \tag{2.16}$$

The effective potential of an impurity is written as

$$V = \begin{pmatrix} u_A(r) & 0 & e^{\imath\eta}u'_A(r) & 0 \\ 0 & u_B(r) & 0 & -\omega^{-1}e^{-\imath\eta}u'_B(r) \\ e^{-\imath\eta}u'_A(r)^* & 0 & u_A(r) & 0 \\ 0 & -\omega e^{\imath\eta}u'_B(r)^* & 0 & u_B(r). \end{pmatrix} \tag{2.17}$$

where $\omega = \exp(2\pi\imath/3)$. If we use a tight-binding model, we obtain the explicit expressions for the potentials as

$$u_A(r) = \sum_{R_A} g(r - R_A) u_A(R_A)$$

$$u_B(r) = \sum_{R_B} g(r - R_B) u_B(R_B)$$

$$u'_A(r) = \sum_{R_A} g(r - R_A) e^{\imath(K'-K)\cdot R_A} u_A(R_A)$$

$$u'_B(r) = \sum_{R_B} g(r - R_B) e^{\imath(K'-K)\cdot R_B} u_B(R_B) \qquad (2.18)$$

where $u_A(R_A)$ and $u_B(R_B)$ are the local site energy at site R_A and R_B, respectively, due to the impurity potential and $g(r)$ is a smoothing function having a range of the order of the lattice constant a and satisfying the normalization condition

$$\sum_{R_A} g(r - R_A) = \sum_{R_B} g(r - R_B) = 1. \qquad (2.19)$$

When the potential range is much shorter than the circumference L, we have

$$u_A(r) = u_A \delta(r - r_A)$$

$$u_B(r) = u_B \delta(r - r_B)$$

$$u'_A(r) = u'_A \delta(r - r_A)$$

$$u'_B(r) = u'_B \delta(r - r_B) \qquad (2.20)$$

with

$$u_A = \frac{\sqrt{3}a^2}{2} \sum_{R_A} u_A(R_A)$$

$$u_B = \frac{\sqrt{3}a^2}{2} \sum_{R_B} u_B(R_B)$$

$$u'_A = \frac{\sqrt{3}a^2}{2} \sum_{R_A} e^{\imath(K'-K)\cdot R_A} u_A(R_A)$$

$$u'_B = \frac{\sqrt{3}a^2}{2} \sum_{R_B} e^{\imath(K'-K)\cdot R_B} u_B(R_B) \qquad (2.21)$$

where r_A and r_B are the centre-of-mass position of the effective impurity potential and $\sqrt{3}a^2/2$ is the area of a unit cell. The integrated intensities u_A, etc given by equation 2.21 have been obtained by the r integral of $u_A(r)$, etc given by equation 2.20.

In the vicinity of $\varepsilon = 0$, we have two right-going channels $K+$ and $K'+$, and two left-going channels $K-$ and $K'-$. The matrix elements are calculated as [27]

$$V_{K\pm K+} = V_{K'\pm K'+} = \frac{1}{2}(\pm u_A + u_B)$$

$$V_{K\pm K'+} = V^*_{K'\pm K+} = \frac{1}{2}(\mp u'_A e^{\imath\eta} - \omega^{-1} e^{-\imath\eta} u'_B). \qquad (2.22)$$

When the impurity potential has a range larger than the lattice constant, we have $u_A = u_B$ and both u'_A and u'_B become much smaller and can be neglected because of the phase factor $e^{\imath(K'-K)\cdot R_A}$ and $\imath e^{\imath(K'-K)\cdot R_B}$. This means that intervalley scattering between K and K' points can be neglected for such impurities as usually assumed in the conventional $\mathbf{k}\cdot\mathbf{p}$ approximation. Further, the above shows that the backward scattering probability within each valley vanishes in the lowest Born approximation.

Figure 11 gives an example of calculated effective potential u_A, u_B and u'_B as a function of d/a for a Gaussian potential located at a B site and having the integrated intensity u. Because of the symmetry corresponding to a 120 rotation around a lattice point, we have $u'_A = 0$ independent of d/a. When the range is sufficiently small, u_B and u'_B stay close to $2u$ because the potential is localized only at the impurity B site. With the increase of d the potential becomes nonzero at neighbouring A sites and u_A starts to increase and at the same time both u_B and u'_B decrease. The diagonal elements u_A and u_B rapidly approach u and the off-diagonal element u'_B vanishes.

This absence of the backward scattering for long-range scatterers disappears in the presence of magnetic fields as shown in figure 12. In high magnetic fields, the intervalley scattering is reduced considerably because of the reduction in the overlap of the wavefunction as shown in equation II A, but the intravalley backward scattering remains nonzero.

The Boltzmann conductivity can be calculated in a straightforward manner by solving a transport equation in a way developed for quantum wires [28]. The conductance in the absence of a magnetic field is always quantized into 2 $e^2/\pi\hbar$ because of the complete absence of backward scattering. With the increase of the magnetic field the conductance is reduced drastically and the amount of the reduction becomes larger with the increase of the length. In strong magnetic fields the conductance becomes nearly independent of the field strength and is roughly proportional to the inverse of the length. This behaviour can be understood by the fact that the conductivity of the 2D graphite is given by 2 $e^2/\pi\hbar$ independent of a magnetic field at $\varepsilon = 0$ and the conductance of the

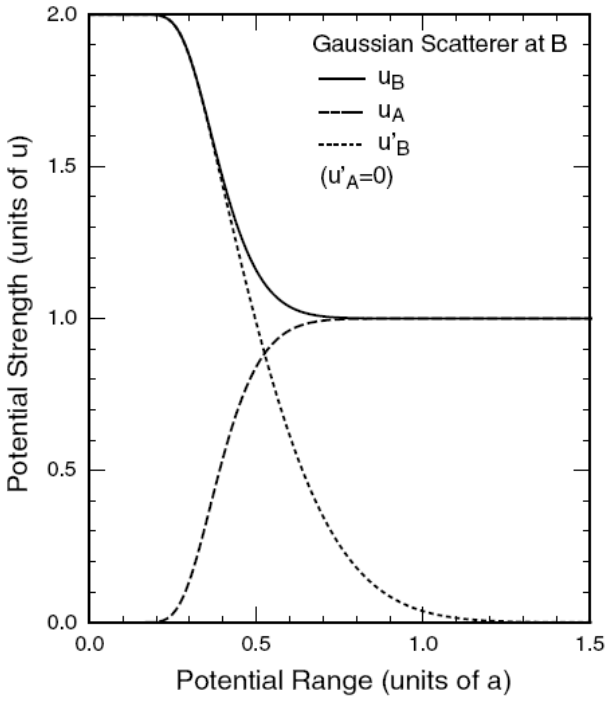

FIG. 11: Calculated effective strength of the potential for a model Gaussian impurity at a B site. After [20].

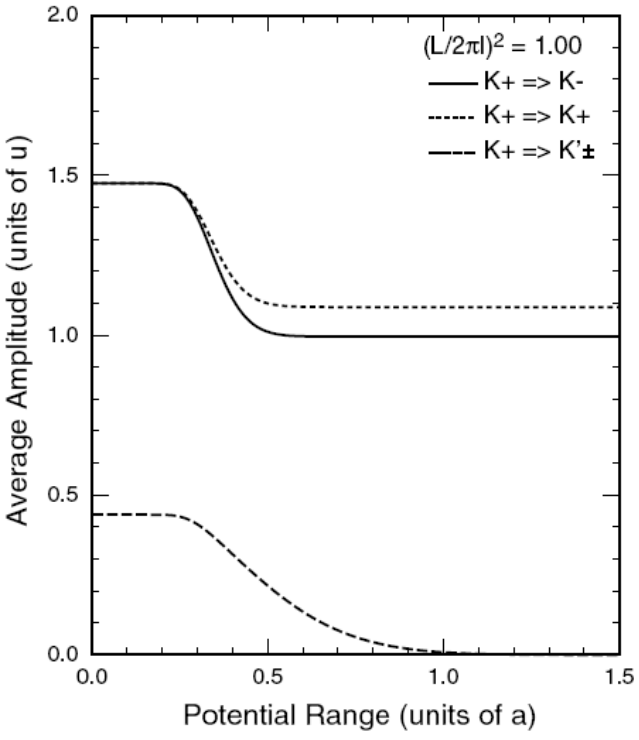

FIG. 12: Calculated effective scattering matrix elements versus the potential range at $\varepsilon = 0$ in the absence of a magnetic field. After [28].

CNT is approximately given by the conductivity of the 2D graphite multiplied by the circumference and divided by the length.

III. KONDO EFFECT IN SINGLE WALLED CARBON NANOTUBES

In the course of this chapter we aim to show the singular Fermi liquid behaviour in 1D, thus leading to a more adequate Luttinger-Tomonaga liquid model. Furthermore, we explain the Kondo effect in the LTL. It is assumed here that the CNT are the physical realisation of the model. Finally, a brief review of the experimental results is presented.

A. Luttinger-Tomonaga behaviour in SWCN

1. *The one-dimensional electron gas*

In this section, we shall outline the special features of the one-dimensional problem which make it soluble and show its singular properties[29]. As it often happens, solubility implies finding the right set of variables in terms of which the Hamiltonian is expressed as a set of harmonic oscillators. In one dimension, the Fermi surface is reduced to the two Fermi points $\mathbf{k} = \pm\mathbf{k}_F$. At low energies, particles may move only to the right or to the left with momenta of almost fixed magnitude $\mathbf{k} \simeq r\mathbf{k}_F$ (belonging, to either the right ($r = 1$) or to the left ($r = -1$) moving branch). Due to the constrained character of one-dimensional motion, the phase space for collisions between particles is severely limited compared to higher dimensions. Let us start by an inspection of the possible collisions. By energy and lattice momentum conservation alone, all the low-energy scattering processes may be classified into four interactions. These interactions are schematically illustrated in figure 13.

By observing this small set of allowed processes we note that the general Hamiltonian describing the low-energy dynamics may be split into four parts

$$H = H_0 + H_{forward} + H_{backward} + H_{Umklapp} \qquad (3.1)$$

In equation 3.1 H_0 is the free electron Hamiltonian

$$H_0 = \sum_k \varepsilon_k c_k^\dagger c_k. \qquad (3.2)$$

The other three terms describe the interactions depicted in figure 13. The Umklapp process ($H_{Umklapp}$), denoted conventionally by H_3 as in fig. 13, describes interactions in which the lattice momentum is conserved yet plain momentum is not: i.e., $k_1^{in} + k_2^{in} = k_1^{out} + k_2^{out} + G$ with $G \neq 0$ a non-vanishing reciprocal lattice vector (a scalar in this one-dimensional case). From fig.13, we note that such a process can occur only in the special case when $4\mathbf{k}_F$ is very close to a reciprocal lattice vector. It

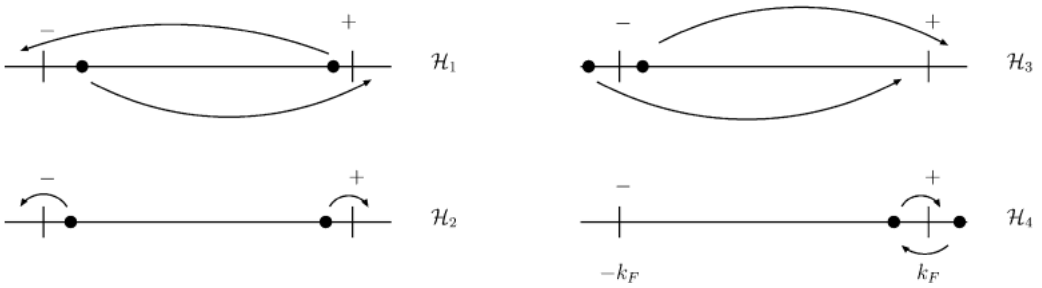

FIG. 13: Pictorial representation of the low-energy interaction terms in the one-dimensional problem. . The + and − points are a shorthand for the two Fermi points $\mathbf{k} = \mathbf{k}_F$ and $(-\mathbf{k}_F)$, respectively. After [30].

follows that except for half-filling of the one-dimensional band, such a process cannot occur. So, in general, one needs to study only forward (H_2 or H_4) processes or backwardscattering (H_1) processes. Note that $H_{forward}$ describes interactions with small momentum transfer and $H_{backward}$ momentum transfer close to $2\mathbf{k}_F$.

We will now introduce a few simplifying assumptions which form the backbone of all Luttinger liquid treatments of the one-dimensional problem:

(1) In eq. 3.2, k may be expanded about the two Fermi points to produce the linear dispersion

$$\varepsilon_r(k) = v_F(rk - k_F) + E_F \tag{3.3}$$

with v_F and E_F denoting the Fermi velocity and the Fermi energy, respectively. As mentioned, $r = \pm 1$ is the right/left branch index.

(2) The band cutoff is taken to be infinite. These assumptions lead us to focus attention on a simplified system in which there are two independent flavors of particles (right and left movers) each of which has a linear dispersion relation with unbounded momentum and energy. The simplified energy spectrum is shown in fig. 14: an infinite sea of unphysical (negative energy) states below the usual Fermi sea. The added infinity of unphysical states with $\varepsilon_k < 0$ have a negligible physical effect (as they are far removed from the chemical potential, they enable the problem to be tractable mathematically).

First we explain how the one-dimensional Hamiltonian can be expressed equivalently in terms of Bosonic variables. Define the charge-density operators ρ_r and the spin-density operators S_r for the two branches, $r = \pm$, by

$$\rho_r = \sum_{\sigma=1} \psi^\dagger_{r,\sigma}\psi_{r,\sigma} \qquad , \qquad S^z_r = \frac{1}{2}\sum_{\sigma,\sigma'} \psi^\dagger_{r,\sigma}\tau^z_{\sigma,\sigma'}\psi_{r,\sigma'}, \tag{3.4}$$

where τ^z is a Pauli matrix. The Fourier transform of the particle-density operators is

$$\rho_{r,\sigma}(q) = \sum_k c^\dagger_{r,\sigma,k+q}c_{r,\sigma,k} = \rho^\dagger_{r,\sigma}(-q). \tag{3.5}$$

A pivotal point is that, within the stated assumptions, these Fermi bilinears may be explicitly shown to obey Bose commutation relations[53].

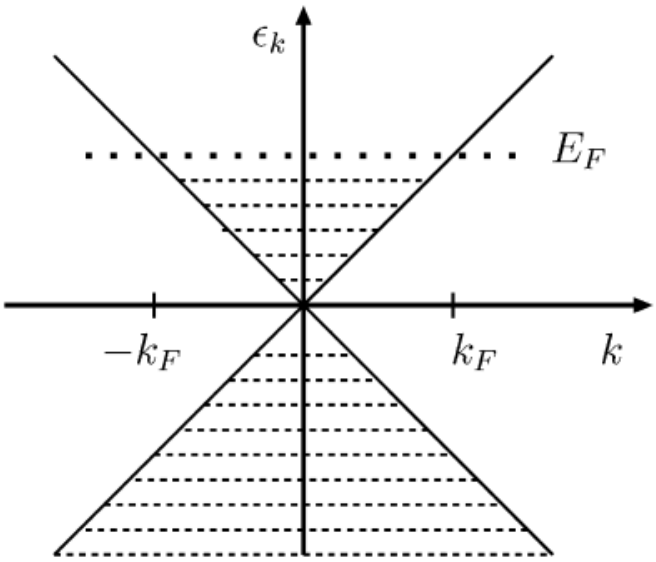

FIG. 14: Single-particle energy ε_k in one dimension, in the approximation that the dispersion relation is linearized about $\mathbf{k}_F$. Note that the Fermi surface consists of just two points. The spectrum of particlehole excitations is given by $\omega(q) = \varepsilon(k+q) - \varepsilon(k) = k_F q = m$. Low-energy particlehole excitations are only possible for q small or for q near $2k_F$. After [29].

We will soon see that these density operators are not merely bosonic but that, in the linear-band approximation, they may also be viewed as raising and lowering operators which reduce the Hamiltonian eq. 3.1 to a simple quadratic (oscillator) form. With our first assumption, we may linearize ε_k about the two Fermi points for low-energy processes; the energy of a particlehole pair created by $\rho_{r,\sigma}(q)$:

$$\varepsilon_{r,k+q} - \varepsilon_{r,k} = rv_F q \tag{3.6}$$

is independent of k in a Luttinger liquid. (This step cannot be implemented in higher dimensions.) In other words, states created by $\rho_{r,\sigma}(q)$ are linear combinations of individual electron hole excitations all of which have the same energy and are therefore eigenstates of H_0. It follows that for $q > 0$, the bosonic $\rho_{r=+,\sigma}(q)[\rho_{r=-}(q)]$ is a raising [lowering] operator. The kinetic energy H_0 may

be expressed in terms of the density operators

$$H_0 = \frac{2\pi v_F}{L} \sum_{r=\pm} \sum_{q>0} \rho_{r,\sigma}(rq)\rho_{r,\sigma}(-rq). \qquad (3.7)$$

Upon separating the densities on a given branch into charge and spin pieces

$$\rho_{r\sigma}(x) = \frac{1}{2}[\rho_r(x) + \sigma S^z_r(x)]$$

the *free Hamiltonian* may be expressed as a sum in the spin and charge degrees of freedom

$$H_0 = \sum_r H_0[\rho_r] + \sum_r H_0[S^z_r].$$

It follows that in the non-interacting problem, spin and charge have identical dynamics and propagate in unison. Once interactions are introduced, the electron will fractionalize and spin and charge dynamics will, in general, differ.

We now turn to a closer examination of the various interaction terms in the Hamiltonian. The part describing the forward scattering (small momentum transfer) events $\rightarrow (k_F, \sigma; k_F, \sigma')$ may be further subdivided (as shown) into the processes $(k_F, \sigma; -k_F, \sigma') \rightarrow (k_F, \sigma; -k_F, \sigma')$ and $(k_F, \sigma; kF, \sigma')$, respectively

$$H_{forward} = H_2 + H_4$$

with

$$H_2 = \frac{1}{L} \sum_q \sum_{\sigma\sigma'} g_2^{\sigma\sigma'} \rho_{+,\sigma}(q)\rho_{-,\sigma'}(-q),$$

$$H_4 = \frac{1}{2L} \sum_q \sum_{\sigma\sigma'} g_4^{\sigma\sigma'} [\rho_{+,\sigma}(q)\rho_{+,\sigma'}(-q) + \rho_{-,\sigma}(q)\rho_{-,\sigma'}(-q)].$$

The operators $\rho_{r,\sigma}$ involve a creation and annihilation operator on the same branch. Let us further define also operators ρ^r_σ formed from bilinears of fermions on opposite branches

$$\rho^r_\sigma = \sum_k c^\dagger_{rr,\sigma,k} c_{-r,\sigma,k+q}.$$

In terms of these, the Hamiltonian describing backscattering interactions (the scattering event $(+k_F, \sigma; -k_F, \sigma') \rightarrow (-k_F, \sigma; k_F, \sigma')$ and its reverse) becomes

$$H_{backwards} = H_1 = g_1 \sum_q \sum_{\sigma\sigma'} g_1^{\sigma\sigma'} \rho^+_\sigma(q)\rho^-_{\sigma'}(-q)$$

and the Umklapp term reads

$$H_{umklapp} = \frac{1}{2L} \sum_q \sum_{\sigma\sigma'} g_3^{\sigma\sigma'} [\rho^+_\sigma(q)\rho^+_{\sigma'}(-q) + \rho^-_\sigma(q)\rho^-_{\sigma'}(-q)].$$

The behaviour of $g_i^{\sigma\sigma'}(q)$ in momentum space translates into corresponding real-space couplings. If the couplings $\{g_i(q)\}$ are momentum independent constants, then the corresponding real-space interactions are local and describe contact collisions. Unless otherwise stated, this is the case that we shall consider.

In all these expressions, the coupling constants may be spin-dependent

$$g_i^{\sigma\sigma'} = g_{i\parallel}\delta_{\sigma\sigma'} + g_{i\perp}\delta_{\sigma\sigma'}. \qquad (3.8)$$

As the terms $H_{1\parallel}$ and $H_{2\parallel}$ describe the same process, we may set $g_{1\parallel} = 0$ with no loss of generality. As already mentioned, Umklapp processes are important only when $4k_F$ is a reciprocal lattice vector so that all scattering particles may be near the Fermi points. The condition for spin rotation invariance $[H, \mathbf{S}] = 0$ reduces the number of independent coupling constants further

$$g_{2\perp} - g_{1\perp} = g_{2\parallel} - g_{1\parallel}.$$

On examining all four possible interactions, we note that the forward scattering H_2 and H_4 break no symmetries but that H_1 and H_3 may. The latter leads to qualitatively new properties. Backscattering breaks the $SU(2)_L \otimes SU(2)_R$ symmetry of spin currents for each of the individual leftright moving fronts. Gaps (or condensates) are usually associated with broken symmetries, and this case is no exception: A spin gap $\Delta_S > 0$ is dynamically generated when these interactions (i.e., an attractive backscattering (H_1) process $(+k_F, \sigma; -k_F, \sigma') \rightarrow (-k_F, \sigma; k_F, \sigma')$).

Similarly, the Umklapp process (H_3) breaks the conservation of individual charge currents; a charge gap $\Delta_c > 0$ is associated with this broken Galilean invariance. The gaps open up only if the interactions are attractive. On a formal level, Umklapp breaks independent right and left $(U(1)_L \otimes U(1)_R)$ charge conservation symmetry leaving the system with only a single $U(1)$ symmetry.

Before discussing the Tomonaga-Luttinger exact solution of the above general model, it is good to obtain physical insight through a phase diagram obtained by the perturbative renormalization group flow equations [31]. Due to the limitation of phase space, the one-dimensional problem is subject to all manners of competing singularities. In one dimension, there are no truly ordered phases of course, but at $T = 0$ correlation functions diverge and one may say that there is algebraic long-range order. One may thus determine a phase diagram according to which susceptibilities diverge as $T \rightarrow 0$: the one associated with singlet superconductivity (SS), triplet superconductivity (TS), a charge-density wave (CDW) at $2k_F$, and a spin-density wave (SDW) at $2k_F$.

2. *The Luttinger-Tomonaga liquid (LTL)*

With forward scattering alone in 3.1 and after linearizing the kinetic energy, we obtain the Luttinger-Tomonaga

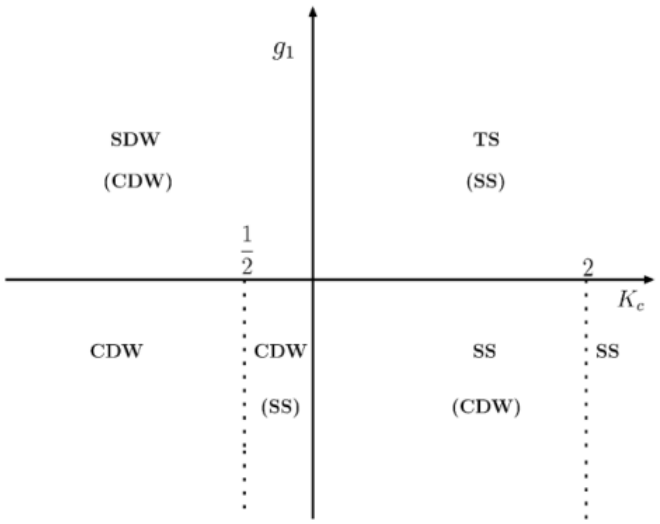

FIG. 15: Phase diagram for one-dimensional interacting fermions in the (K_c, g_1) plane with $g_{1\parallel} = 0$ in eq.3.8 and K_c given by eq. 3.12. *SDW* and *CDW* in the upper left quadrant indicates that both the spin density wave susceptibility and the charge-density wave susceptibility diverge as $T \to 0$, but that the spin-density wave susceptibility diverges a factor $\ln^2 T$ faster than the charge-density wave susceptibility [29]. Other sectors are labelled accordingly. After [29].

(L-T) model. In terms of fermion field operators $\psi_{r,\sigma}(x)$ and $\psi^\dagger_{r,\sigma}(x)$ and density and spin operators $\rho_r(x)$ and $S^z_r(x)$ in real space, the L-T model is

$$H^{L-T} = \int dx \left[-v_F \sum_{r,\sigma=\pm} r\psi^\dagger_{r,\sigma} \imath\partial_x \psi_{r,\sigma} + \frac{1}{2}\sum_{r=\pm} g_{2,c}\rho_r(x)\rho_{-r}(x) \right] + \sum_{r=\pm} g_{4,c}\rho_r(x)\rho_r(x) + 2\sum_{r=\pm} g_{2,s} S^z_r(x) S^z_{-r}(x) + g_{4,s} S^z_r(x) S^z_r(x), \tag{3.9}$$

where

$$g^c_i = \frac{g_{i\parallel} + g_{i\perp}}{2} \quad , \quad g^s_i = \frac{g_{i\parallel} - g_{i\perp}}{2} \tag{3.10}$$

Note that the $g_{2,s}$ term is the only term which breaks $SU(2)$ spin symmetry. The L-T model is exactly solvable. After all, as previously noted, the (Dirac-like) kinetic energy Hamiltonian H_0 is also quadratic in the density operators. So the Hamiltonian is readily diagonalized by a Bogoliubov transformation whereupon the Hamiltonian becomes a sum of two independent (harmonic) parts describing non-interacting charge- and spin-density waves: the charge- and spin-density waves are the collective eigenmodes of the system. The simplest way to solve the LT model and to explicitly track down these collective modes is via the bosonization of the electronic degrees of freedom. The bosonic representation of the fermionic fields proceeds by writing [32].

$$\psi_{r,\sigma}(x) = \lim_{a\to 0} \frac{\exp\left[\imath r(k_F x + \Phi_{r\sigma}(x))\right]}{\sqrt{2\pi a}} F_{r\sigma}$$

where a is a short distance regulator. $\Phi_{r\sigma}(x)$ satisfies

$$[\Phi_{r,\sigma}(x), \Phi^\dagger_{r',\sigma'}(x)] = -\imath\pi\delta_{r,r'}\delta_{\sigma,\sigma'}\mathrm{sign}(x - x').$$

The so-called Klein factors[54] $F_{r,\sigma}$ are chosen such that the proper fermionic anticommutation relations are reproduced. The exponential envelope $\exp[\imath\Phi_{r,\sigma}(x)]$ represents the slow bosonic collective degrees of freedom which dress the rapidly oscillating part $F_{r,\sigma}\exp(\imath k_F x)$ describing the energetic particle excitations near the Fermi points.

The slowly varying fields Φ may be written in terms of the bosonic fields $\phi_{c,s}$ and their conjugate momenta $\partial_x\theta_{c,s}$

$$\Phi_{r,\sigma} = \sqrt{\pi/2}\left[(\theta_c - r\phi_c) + \sigma(\theta_s - r\phi_s)\right]$$

In terms of the new variables, the familiar charge and spin densities are

$$\rho(x) = \sum_r \rho_r(x) = \sqrt{\frac{2}{\pi}}\partial_x\phi_c \quad ,$$
$$S^z(x) = \sum_r S^z_r(x) = \sqrt{\frac{1}{2\pi}}\partial_x\phi_s.$$

In the $(\theta_{c,s}, \phi_{c,s})$ representation, the Luttinger-Tomonaga Hamiltonian becomes a sum of two decoupled sets of oscillators describing the gapless charge and spin density wave eigenmodes

$$H^{L-T} = \int dx \sum_{\nu=c,s} \frac{v_\nu}{2}\left[K_\nu(\partial_x\theta_\nu)^2 + \frac{(\partial_x\theta_\nu)^2}{K_\nu}\right] \equiv H_s^{L-T} + H_c^{L-T}. \tag{3.11}$$

The parameters K_c and K_s are the LTL parameters controlling charge and spin sectors, respectively. Roughly speaking, they are smaller (larger) than unity when densitydensity interactions are repulsive (attractive). For noninteracting electrons $K_c = K_s = 1$. For example, in the Hubbard model with on-site repulsion U the parameter K_c decreases from 1 to 1=2 as U increases from 0 to infinity. With longer-range interactions K_c can take a value smaller than 1/2. It is also important to note that, when the Hamiltonian has $SU(2)$ spin rotation symmetry, K_s is renormalized to 1 in the low-energy limit.

The velocities of the collective charge and spin modes are easily read of by analogy to a harmonic string

$$v_{c,s} = \sqrt{\left(v_F + \frac{g_4^{c,s}}{\pi}\right)^2 - \left(\frac{g_2^{c,s}}{\pi}\right)^2}.$$

Likewise, the moduli determining the power-law decay of the correlations are

$$K_{c,s} = \sqrt{\frac{\pi v_F + g_4^{c,s} - g_2^{c,s}}{\pi v_F + g_4^{c,s} + g_2^{c,s}}}. \tag{3.12}$$

The above expressions for the spin and charge density wave velocities simply follow from the conservation of left and right moving particles in the L-T model. As previously noted, the charge and spin velocities are degenerate in the non-interacting model. When interactions are introduced, the charge and spin velocities (v_c and v_s) as well as the energy to create spin and charge excitations (v_s/K_s and v_c/K_c, respectively) become different. The charge constant K_c is less than 1 for repulsive interactions, which elevates the energy of the charge excitations, while K_c is greater than 1 for attractive interactions.

From equation 3.11, some thermodynamic quantities can be derived. As evident from this expression the contributions of the independent charge and spin modes must appear independently in most physical quantities. The specific heat coefficient is found to be

$$\gamma/\gamma_0 = \frac{v_F}{2}\left(\frac{1}{v_c} + \frac{1}{v_s}\right),$$

where $\gamma = \gamma_0$ for the non-interacting system.

The spin susceptibility and the compressibility are also readily computed from 3.11

$$\chi_0 = v_F/v_s \quad , \kappa/\kappa_0 = v_F K_c/v_c$$

where χ_0 and κ_0 are the susceptibility and compressibility of the non-interacting gas.

An important theoretical result is that compared to a non-interacting resonant level at the chemical potential, the ratio of the magnetic susceptibility enhancement to the specific heat enhancement

$$R_W = \frac{\delta\chi/\chi}{\delta C_v/C_v} \tag{3.13}$$

for spin 1/2 impurities at $T \ll T_K$ is precisely 2 [10]. In a non-interacting model, this ratio, nowadays called the Wilson ratio, is equal to 1, since both χ and C_v are proportional to the density of states $N(0)$. Thus, the Wilson ratio is a measure of the importance of correlation effects.

In this case, the Wilson ratio is

$$R_W = \frac{\chi/\chi_0}{\gamma/\gamma_0} = \frac{2v_c}{v_c + v_s} \tag{3.14}$$

It deviates from its Fermi-liquid value of unity by an amount dependent on the relative separation between the spin and charge velocities.

B. Kondo effect in a LTL

Finally, we turn to the Kondo effect of one-dimensional repulsively interacting electrons [33]. Suppose that there is an impurity spin ($S = 1/2$) at the origin. As we have seen in the previous sections, in one dimension we need to distinguish forward and backward scattering by the impurity, unless the impurity spin is at the boundary. We thus consider two kinds of Kondo exchange couplings: forward Kondo scattering J_F and backward Kondo scattering J_B [33, 34]. The Kondo scattering is described by

$$H_J = \frac{J_F}{2}\mathbf{S}\left[\psi^\dagger_{R\sigma}(0)\tau_{\sigma\sigma'}\psi_{R,\sigma}(0) + \psi^\dagger_{L\sigma}(0)\tau_{\sigma\sigma'}\psi_{L,\sigma}(0)\right] + \frac{J_B}{2}\mathbf{S}\left[\psi^\dagger_{R\sigma}(0)\tau_{\sigma\sigma'}\psi_{L,\sigma}(0) + \psi^\dagger_{L\sigma}(0)\tau_{\sigma\sigma'}\psi_{R,\sigma}(0)\right] \tag{3.15}$$

where we now denote by R/L the right/left moving particles, replacing the previous notation $(r = +)/(r = -)$. Again, $\tau = (\tau^x, \tau^y, \tau^z)$ are Pauli matrices.

We assume that the bulk LTL is described by the Hamiltonian H^{L-T} 3.11, where the SU(2) spin rotation symmetry implies $K_s = 1$. The electron-electron interaction is weak and repulsive $g_2 < 0$, so that the parameter $K_c = [(1 - g_2/\pi v_F)/(1 + g_F/\pi v_F)]^{1/2}$ determining the zero-temperature correlation exponents in LTL impurity free is less than 1. The bare Kondo couplings satisfy the relation $J_{\perp F} = J_{zF} = J_{\perp B} = J_{zB} = J_0$, implying that the impurity spin also has $SU(2)$ symmetry. An important feature of this model presented by Furusaki and Nagaosa [34] is that there exist two kind of Kondo coupling, forward scattering ($J_{\perp F}$ and J_{zF}) and backward scattering ($J_{\perp B}$ and J_{zB}), in contrast to the Kondo problem in 3D, in which case after some transformations we have only left-going electrons scattered by forward Kondo couplings (section I). The Kondo scattering 3.15 can be bosonized as in III A 2. The forward Kondo scattering term can be expressed with the spin boson only [35], while the backward Kondo scattering term involves both charge and spin bosons The existence of the latter coupling is essential to the current discussion.

We first study the weak-coupling regime in which $g_2/\pi v_F \ll 1, J_{\perp F(B)}/\pi v_F \ll 1$ and $J_{zF(B)}/\pi v_F \ll 1$. Up to one-loop order, renormalization-group equations can be easily derived using, for example, the poor-man's scaling method[9]. Up to the order $g_2 J$ and J^2, the scaling equations read

$$\frac{dJ_{\perp F}}{dl} = \frac{1}{2\pi v_F}(J_{\perp F}J_{zF} + J_{\perp B}J_{zB}) \tag{3.16}$$

$$\frac{dJ_{zF}}{dl} = \frac{1}{2\pi v_F}(J_{\perp F}^2 + J_{\perp B}^2) \tag{3.17}$$

$$\frac{dJ_{\perp B}}{dl} = \frac{1}{2\pi v_F}(g_2 J_{\perp B} + J_{\perp F}J_{zB} + J_{\perp B}J_{zF}) \tag{3.18}$$

$$\frac{dJ_{zB}}{dl} = \frac{1}{2\pi v_F}(g_2 J_{zB} + 2J_{\perp F}J_{\perp B}), \tag{3.19}$$

where $dl = -d\ln W_c$ with W_c being the bandwidth cutoff. We note that the above equations preserve the SU(2) symmetry, and thus we may set $J_{\perp F} = J_{zF} = J_F$ and $J_{\perp B} = J_{zB} = J_B$. The scaling dimension of magnetic impurity scattering is the same as that of nonmagnetic impurity scattering. Thus, the scaling dimension of J_F is one, whereas J_B has dimension $(1 + K_c)/2$, and the equations are reduced to

$$\frac{dJ_F}{dl} = \frac{1}{2\pi v_F}(J_F^2 + J_B^2) \tag{3.20}$$

$$\frac{dJ_B}{dl} = \frac{1}{2}(1 - K_c)J_B + \frac{1}{\pi v_F}J_F J_B. \tag{3.21}$$

A schematic flow diagram is shown in figure 16.

The flow diagram tells that the trivial fixed point $J_F = J_B = 0$ becomes unstable with infinitesimal J_B, because the backward scattering is relevant for $K_c < 1$. This leads to a somewhat surprising conclusion that the Kondo couplings are renormalized towards strong couplings, no matter whether the Kondo couplings are antiferromagnetic or ferromagnetic. This should be contrasted with

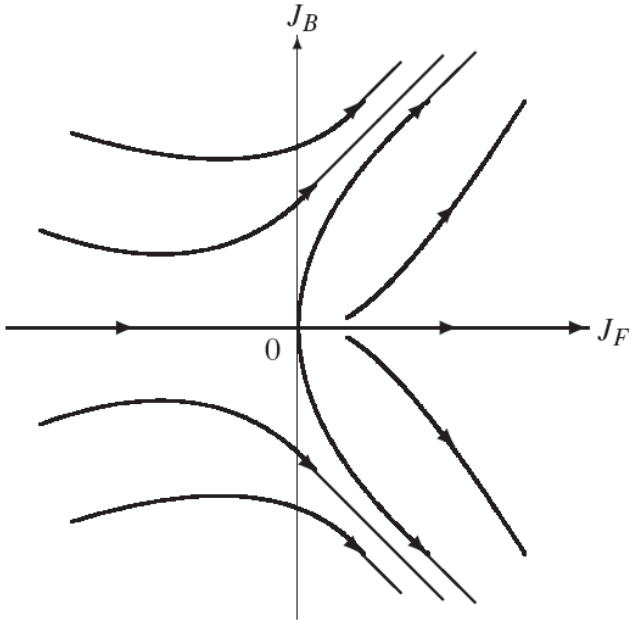

FIG. 16: Schematic flow diagram for the Kondo couplings for the $K_c < 1$ and $K_s = 1$. After [33]

.

the standard Fermi liquid case in which the Kondo coupling is renormalized to the strong-coupling regime only if it is anti- ferromagnetic. Another point to note is that the Kondo temperature depends on the Kondo coupling constant not exponentially but algebraically in LTLs.

The one-loop scaling equations 3.20 and 3.21 suggest three fixed points besides the trivial one, $(J_F, J_B) = (0, 0)$, mentioned above. These three are $(J_F, J_B) = (+\infty, +\infty)$, $(+\infty, 0)$ and $(+\infty, -\infty)$.

Let us first discuss the case $J_B = 0$. In this case the charge and spin sectors are decoupled in the bosonized Hamiltonian $H^{L-T} + H_J$. The impurity spin is interacting with ϕ_s and θ_s only, and the Hamiltonian of the spin sector is equivalent to that of the two-channel Kondo problem [35]. Here the right- and left-going electrons correspond to two channels. As is well known, the ferromagnetic coupling $J_F > 0$ is renormalized to zero, while the antiferromagnetic coupling flows to the strong-coupling fixed point of the two-channel Kondo model. In the latter case the specific heat and the spin susceptibility acquire anomalous logarithmic contributions due to a local leading irrelevant operator with dimension 3/2 at the strong-coupling fixed point:

$$\delta C \propto T\ln(T_K/T) \quad , \quad \delta\chi \propto \ln(T_K/T). \tag{3.22}$$

Since the charge excitations have the velocity v_c which is different from the spin velocity v_s, the Wilson ratio is slightly modified from the standard result 8/3 to

$$R_W = \frac{4}{3}\left(1 + \frac{v_s}{v_c}\right) \tag{3.23}$$

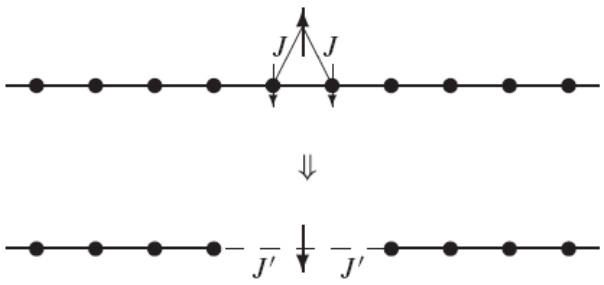

FIG. 17: Lattice model in which an impurity spin is coupled antiferromagnetically to two lattice sites. After [33]

.

A simple lattice model realizing this two-channel Kondo physics is depicted in figure 17, where an impurity spin $S = 1/2$ is coupled to two neighbouring sites with equal antiferromagnetic Kondo coupling J. When the electron density is at half filling, one can easily show that the backward scattering vanishes in the continuum limit[34].

Since the charge sector is gapped at half filling, the model is essentially the same as the antiferromagnetic Heisenberg chain with the impurity spin [36, 37]. We now turn our attention to the generic case $J_F J_B \neq 0$. Since the Kondo couplings always flow towards strong couplings (fig. 16), it is natural to assume that in the ground state the impurity spin is completely screened as in the standard Kondo effect in Fermi liquids (an exception is the two-channel Kondo case discussed above, which requires the condition $J_B = 0$). We can thus draw schematic strong- coupling pictures of the stable fixed points for (a) anti- ferromagnetic and (b) ferromagnetic Kondo couplings; see fig. 18. The ground state consists essentially of two semi- infinite LTLs and a singlet in between them. Since the isolated singlet is expected to have a finite energy gap to excited states, these pictures suggest that the low-energy effective theory is given by two decoupled semi-infinite LTLs plus residual perturbations. Before concluding that these pictures are indeed correct, we have to examine whether the residual interactions are irrelevant at the fixed points. Local operators that could be generated during the renormalization group transformation are the local potential operator at the two ends of the LTLs and the single-electron tunneling between the LTLs. They can be generated by virtual breaking of the singlet due to electron hopping into or out of the singlet. Denoting the end sites of the left and right semi-infinite LTLs by l and r, respectively, we can write these operators as $\psi^\dagger_\sigma(l)\psi_\sigma(l)+\psi^\dagger_\sigma(r)\psi_\sigma(r)$ and $\psi^\dagger_\sigma(l)\psi_\sigma(r)+\psi^\dagger_\sigma(r)\psi_\sigma(l)$ where summation over the spin index σ is assumed. The former is exactly marginal and can lead to a shift of the ground state energy. The latter operator is equivalent to the single-electron tunneling. It has scaling dimension $(K_c^{-1}+1)/2$ at $K_s = 1$ and is irrelevant in the repulsively interacting electrons ($K_c < 1$). We can thus safely conclude that the strong-coupling fixed points are basically two decoupled semi-infinite LTLs, and the impurity spin is completely screened and disappears from the low-energy theory. Treating the tunneling operator as a perturbation, we can compute the impurity contributions to the specific heat and the spin susceptibility at low temperatures. The results are [34]

$$\delta C = c_1(K_c - 1)^2 T^{1/K_c - 1} + O(T), \quad (3.24)$$

$$\delta\chi = c_2 + O(T), \quad (3.25)$$

where c_1 and c_2 are positive constants. When $1/2 < K_c < 1$, which is the case in the Hubbard model, the low-temperature specific heat has the anomalous power-law contribution as a leading term. This result is confirmed by the boundary conformal field theory analysis as well as by a quantum Monte Carlo calculation[38]. The XXZ spin chain with an extra impurity spin also shows a similar temperature dependence[39]. If the single-electron tunneling operator is not allowed by symmetry (particle-hole symmetry), then $c_1 = 0$ and the low-temperature behaviour is Fermi-liquid like. This is probably what is happening in the solvable toy model studied by Schiller and Ingersent. [40]

One can also think of the possibility of having a static impurity potential in addition to the magnetic impurity. This is indeed what one would find if one takes the asymmetric Anderson model. Fabrizio and Gogolin [41] argued that, if $K_c < 1/2$ and if the static potential is sufficiently strong, then a situation similar to the one drawn in fig. 17 occurs and the two-channel Kondo physics is realized. Quantum Monte Carlo calculations [42] have obtained results that are consistent with this scenario.

Recent studies have shown that this is not the whole story. [43]. The discussed low-energy theory of a LTL is the Gaussian model H^{T-L} perturbed by a marginally irrelevant operator $\cos(2\phi_\sigma)$. Even though it is renormalized to zero in the low-energy limit, it should be included in the calculations of finite-temperature quantities like the specific heat and the susceptibility. At the strong- coupling fixed point (fig. 18) where the impurity spin is completely screened, the field obeys a Dirichlet boundary condition at the end sites. As a consequence the first-order perturbation $\langle\cos(2\phi_\sigma)\rangle$ gives a nonvanishing contribution to the free energy. That contribution comes from the region localized near the end sites within the distance of order v_s/T. This boundary contribution turned out to give leading contribution in δC and $\delta\chi$,

$$\delta C = \frac{1}{2\left[\ln(T_K/T)\right]^2}, \quad (3.26)$$

$$\delta\chi = \frac{1}{12T\ln(T_K/T)}, \quad (3.27)$$

where T_K is the Kondo temperature for the bulk marginally irrelevant operator, while the coefficients $1/2$ and $1/12$ are universal. The low-temperature behaviour 3.26 should be easily observed when the impurity poten-

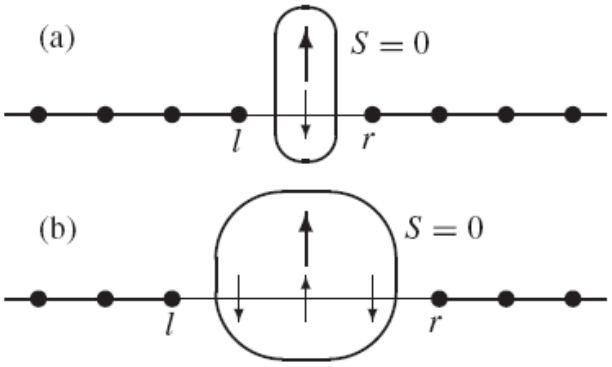

FIG. 18: Schematic pictures of the strong-coupling fixed points for (a) antiferromagnetic and (b) ferromagnetic Kondo couplings After [33]

.

tial is sufficiently strong so that the strong-coupling fixed point is already reached at T_K.

C. Experimental studies on SWCN

Recent advances in nanotechnology enabled scientist to access experiments on a scale of just a few nanometers. SWNTs provide exciting opportunities to study other fundamental issues in 1D electron hosts. For example, the availability of SWNTs enables one to probe how 1D electron systems interact with magnetic impurities, that is, the Kondo effect in 1D. Moreover, the SWNT have been shown to act as Luttinger-Tomonaga liquid(LTL).

Measurements of the resistance of a single multi-wall nanotube were reported, and irregular oscillation analogous to universal conductance fluctuations was observed [44]. A resistance oscillation more regular like that of an Aharonov-Bohm type was observed in a magnetic field parallel to the CNT axis [45]. Recently observed resistance oscillation in a parallel field was shown to be consistent with the Aharonov-Bohm oscillation of the bandgap due to a magnetic flux passing through the CNT cross section [46].

Because of the presence of large contact resistance between a nanotube and metallic electrode, the measurement of the conductance of a nanotube itself is quite difficult. However, from measurements of single-electron tunnelling due to a Coulomb blockade and charging effect, important information can be obtained on the effective mean free path and the amount of backward scattering in nanotubes. Discrete quantized energy levels were measured for a nanotube with 3 μm length, for example, showing that the electron wave is coherent and extended over the whole length.

It was shown further that the Coulomb oscillation in semiconducting nanotubes is quite irregular and can be explained only if nanotubes are divided into many separate spatial regions in contrast to that in metallic nanotubes [47]. This behaviour is consistent with the presence of a considerable amount of backward scattering leading to a strong localization of the electron wave function in semiconducting tubes. In metallic nanotubes, the wave function is extended throughout the whole region of a nanotube because of the absence of backward scattering.

A conductance quantization was observed in multi-wall nanotubes [48]. This quantization is likely to be related to the absence of backward scattering shown here, but much more work is necessary including effects of magnetic fields and problems related to contacts with a metallic electrode before complete understanding of the experimental result. At room temperature, where the experiment was performed, phonon scattering is likely to play an important role.

1. *Evidence of LTL behaviour in CNT*

Due to the small sample size, boundary conditions become of importance, and may dominate the physics. As argued before, for a quantum wire, the conductance is given by $G_n = 2nK_\rho e^2/h$ where n is the number of conducting channels. When the wire is coupled to Fermi liquid leads, however, the interaction renormalization is absent, and $G_n = 2ne^2/h$ a boundary effect.

The influence of isolated impurities on transport, or tunneling through quantum point contacts, is an important problem. At higher temperatures (voltages), there will be corrections to the (differential) conductance $\delta G \sim T^{K_c-1}$, respectively $\delta(dI/dV) \sim V^{K_c-1}$. With repulsive interactions and at low energy scales, an impurity will cut the quantum wire into two segments with only a weak link between them. In this case, the conductance, respectively differential conductance, vary as $G(T)\ T^{K_c^{-1}-1}$, resp. $dI/dV\ V^{K_c^{-1}-1}$. The physical origin of this effect, nameley strong oscillation around the impurity which will increasingly backscatter the electrons at lower energy scales, has been discussed in section III A 2.

An impurity can therefore be assimilated with open boundary conditions. This identifies the exponents just described as members of a larger class of boundary critical exponents. Quite generally, 1D interacting fermions with open boundaries and gapless excitations form a bounded Luttinger liquid state, rather similar to ordinary Luttinger liquids but with a different set of exponents and scaling relations. The K_ν are properties of the Hamiltonian, and therefore independent of boundary conditions. The correlation functions, and their exponents, however depend on boundary conditions. A particularly nice experiment demonstrating this relation, has been performed on carbon nanotubes [49]. With different preparations, it is possible to tunnel electrons from electrodes either into the end of nanotubes, or into their bulk. In the first case, conductance and differential conductance measure the power-laws just described for tun-

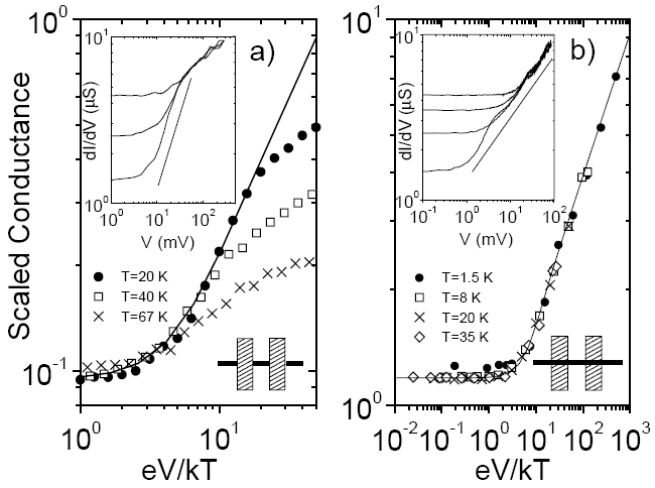

FIG. 19: The differential conductance dI/dV measured at various temperatures. Figure 3a inset: dI/dV curves taken on a bulk-contacted rope at temperatures T=1.6 K, 8 K, 20 K, and 35K. Figure 3b inset: dI/dV curves taken on an end-contacted rope at temperatures T=20 K, 40 K, and 67 K. In both insets, a straight line on the log-log plot is shown as a guide to the eye to indicate power-law behaviour. The main panels show these measurements collapsed onto a single curve using the scaling relations described in the text. The solid line is the theoretical result fit to the data using γ as a fitting parameter. The values of γ resulting in the best fit to the data are $\gamma = 0.46$ in (a) and $\gamma = 0.63$ in (b). After [49].

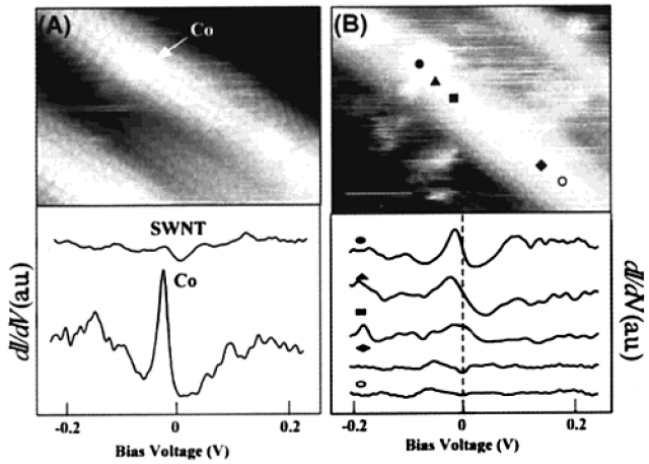

FIG. 20: (A) Atomically resolved image of a 0.5 nm Co cluster on a SWNT, and dI/dV versus V recorded at the position of the Co cluster and $\sim$ 7 nm away from the cluster. (B) Constant current image of a larger Co cluster ($\sim$1 nm) on a SWNT, and corresponding dI/dV versus V measured at points indicated in the image. Figure from [22].

neling through a weak link, while for tunneling into the bulk, they measure the bulk density of states, described in the context of photoemission. The exponents differ slightly from those given here because of the peculiar band structure of the tubes and because the electrons tunnel from a Luttinger liquid into a normal metal(see figure 19). The remarkable result of this work is that the various experiments can be described in terms of a single coupling constant $K_\nu \sim 0.28$.

2. *Studies of the Kondo effect in CNT*

Kondo effect has been first observed in CNT by Nygard et al. [50]. Due to the finite length, given the lithographically fabricated contacts on opposites sides of the CNT (two-terminal device with source and drain contacts), the one-dimensional CNT is turned into a quantum dot [51] at low temperatures (typically at $\lesssim 10K$), a zero dimensional object with a discrete level spectrum. The confinement is formed by the finite back-reflection at the edges of the contacts.

As we have seen, the CNT exhibit four-fold degeneracy of the shells. This four-fold degeneracy has been observed by Bockrath et al. [49] in SWNTs. Singlet-triplet transitions mix these degenerate states, and are thought to account for conductance anomalies observed in the CNTs. The first measurements which reported the Kondo effect in CNTs were made with an STM near cobalt clusters that were deposited on the nanotubes. [50]

Odom et al. [52] first studied the interaction between the local spin of Co clusters and extended and finite size SWNTs. STM images showed that Co clusters could be readily observed on atomically resolved metallic SWNT (Figure 20), and spectroscopy data recorded directly above the cluster exhibited a strong resonance peak near E_F. Spatially resolved measurements further showed that these peak features systematically decrease in amplitude and ultimately disappear after several nanometers. The new resonance peaks were not observed with nonmagnetic Ag clusters or with Co clusters on semiconducting SWNTs,[52] which suggested that the observed peak was due to the interaction of a magnetic spin with the SWNT conduction electrons. In addition, analyses of the resonance revealed new characteristics about the effect of dimensionality compared with 2D systems. In 2D systems, the Kondo resonance is usually evident as a dip or antiresonance in the tunneling conductance, while in the measurement of Co on SWNTs, the Kondo resonance always appears as a sharp peak. This difference can be qualitatively understood in terms of the small number of "continuum" final states available for tunneling into a SWNT versus a noble metal surface in this two-channel quantum interference problem.

Odom et al.[13] also studied the Kondo effect in a very short metallic SWNT, where the energy level spacing of the conduction electrons was larger than $k_B T_K$ (vs normally $k_B T_K$ in extended systems), by characterizing the DOS on and near Co clusters before and after cutting a SWNT host to 11 nm. The spectra recorded after cutting not only resolved the expected discrete eigenstates separated by $\sim$0.15 eV, due to the quantum finite size ef-

fect, but also showed that the peak amplitude at E_F was markedly enhanced relative to those of the other level peaks. The enhanced conductance at E_F provides evidence of how sensitive the electronic properties of metallic nanotubes are to magnetic impurities, even in finite size structures where the level spacing is much larger than $k_B T_K$.

These initial studies suggest that metallic SWNTs are ideal hosts for studying the basic physics of the Kondo effect in 1D systems, although the magnetic clusters (< 1 nm) explored in this first report also complicate analysis compared to the ideal of a single atom spin centre. In this regard, future studies of the 1D Kondo effect could benefit substantially by using single magnetic atoms or molecules that have well-defined (and controllable) spin and can be registered precisely with respect to the underlying SWNT atomic lattice.

IV. CONCLUSIONS AND PERSPECTIVES

In this review we have focused on the occurrence of Kondo effect in carbon nanotubes.

Kondo's explanation of the resistance minimum in a metal with magnetic impurities has been followed, showing an example where second order terms in perturbation theory become of crucial importance for understanding the physical phenomenon.

Electronic properties of carbon nanotubes have been discussed theoretically based on a $\mathbf{k} \cdot \mathbf{p}$ scheme. The motion of electrons of electrons in carbon nanotubes give rise to interesting effects, such as Aharonov-Bohm on the bandgap, the absence of back scattering and the conductance quantization in presence of scatterers with a potential range larger than the lattice constant.

A metallic CNT has energy bands having a linear dispersion in the vicinity of the Fermi level and therefore is expected to provide an Luttinger-Tomonaga liquid — an ideal one-dimensional system where important electron-electron interaction effects come into play and can be studied. In a LTL the bosonization technique leads to spin-charge separation, giving rise to different contributions to physical quantities.

The first experiments seem to confirm that CNT act indeed as a LTL, having obtained a qualitatively power-law dependence of conductance of temperature and applied voltage. But still, there is room for further investigations, which could also provide quantitative results.

As we have seen, the quantum impurity problems in LTLs share many interesting features with the Kondo problem. Some of the theoretical predictions for the simplest case of a static impurity have been confirmed by tunneling experiments on carbon nanotubes.

Investigations into the Kondo effect are far from complete. An example of ongoing debate concerns the so-called Kondo cloud. The electrons which have interacted with the same magnetic impurity are considered mutually correlated. The question is if we can measure and control the Kondo cloud and understand how this state build up.

New physical phenomena can emerge in the study of molecular nanostructures. Further efforts promise to be rewarded with answers to very fundamental questions and importantly, these results could push further the applications in future nanotechnologies.

Acknowledgments

I would like to thank my advisor Maxim Mostovoy for his stimulating help and constant support. Through his sharp insight and amount of knowledge he sets a high level for his students and collaborators, challenging them continuously. But due to his willingness to help and to share his knowledge he brings them closer to see the beauty of theoretical physics.

[1] L. Kouwenhoven and L. Glazman, Physics World **14**, 33 (2001).
[2] J. Kondo, Progress Of Theoretical Physics **32**, 37 (1964).
[3] W. J. de Haas, J. de Boer, and G. J. van den Berg, Physica **1**, 1115 (1934).
[4] O. Taylor, Philip L.; Heinonen, *A Quantum Approach to Condensed Matter Physics* (Cambridge University Press, 2002).
[5] J. Kondo, Journal Of The Physical Society Of Japan **74**, 1 (2005).
[6] S. V. Vonsovsky, Zhurnal Eksperimentalnoi I Teoreticheskoi Fiziki **16**, 981 (1946).
[7] J. R. Schrieffer and P. A. Wolff, Physical Review **149**, 491 (1966).
[8] P. W. Anderson, Physical Review **1**, 41 (1961).
[9] P. W. Anderson, Journal Of Physics Part C Solid State Physics **3**, 2436 (1970).
[10] K. G. Wilson, Reviews Of Modern Physics **47**, 773 (1975).
[11] N. E. Bickers, D. L. Cox, and J. W. Wilkins, Phys. Rev. Lett. **54**, 230 (1985).
[12] S. Iijima, Nature **354**, 56 (1991).
[13] T. W. Odom, J. L. Huang, P. Kim, and C. M. Lieber, Nature **391**, 62 (1998).
[14] J. W. Mintmire, B. I. Dunlap, and C. T. White, Physical Review Letters **68**, 631 (1992).
[15] A. T. Ajiki H., J. Phys. Soc. Japan **62**, 2470 (1992).
[16] A. T. Ajiki H., Japan J. Appl. Phys. Suppl. **34**, 107 (1995).
[17] T. Ando, J. Phys. Soc. Japan **66**, 1066 (1996).
[18] N. A. Viet, H. Ajiki, and T. Ando, Journal Of The Physical Society Of Japan **63**, 3036 (1994).
[19] H. Ajiki and T. Ando, Journal Of The Physical Society Of Japan **64**, 4382 (1995).
[20] T. Ando, Semiconductor Science And Technology **15**, R13 (2000).

[21] P. R. Wallace, Physical Review **71**, 622 (1947).

[22] M. Ouyang, J. L. Huang, and C. M. Lieber, Accounts Of Chemical Research **35**, 1018 (2002).

[23] W. Tian and S. Datta, Phys. Rev. B **49**, 5097 (1994).

[24] J. W. McClure, Phys. Rev. **119**, 606 (1960).

[25] D. E. Soule, J. W. McClure, and L. B. Smith, Phys. Rev. **134**, A453 (1964).

[26] T. Ando and T. Seri, J. Phys. Soc. Japan **66**, 3558 (1997).

[27] T. Ando and T. Nakanishi, Journal of the Physical Society of Japan **67**, 1704 (1998).

[28] H. Akera and T. Ando, Phys. Rev. B **43**, 11676 (1991).

[29] C. M. Varma, Z. Nussinov, and W. van Saarloos, Physics Reports-Review Section Of Physics Letters **361**, 267 (2002).

[30] W. Metzner, C. Castellani, and C. Di Castro, Advances In Physics **47**, 317 (1998).

[31] J. Solyom, Advances In Physics **28**, 201 (1979).

[32] N. Nagaosa, *Quantum field theory in Strongly Correlated Electronic Systems* (Springer, 1999).

[33] A. Furusaki, Journal Of The Physical Society Of Japan **74**, 73 (2005).

[34] A. Furusaki and N. Nagaosa, Physical Review Letters **72**, 892 (1994).

[35] I. Affleck and A. W. W. Ludwig, Nuclear Physics B **360**, 641 (1991).

[36] S. Eggert and I. Affleck, Physical Review B **46**, 10866 (1992).

[37] D. G. CLARKE, T. GIAMARCHI, and B. I. SHRAIMAN, Physical Review B **48**, 7070 (1993).

[38] P. Durganandini, Physical Review B **53**, R8832 (1996).

[39] A. Furusaki and T. Hikihara, Physical Review B **58**, 5529 (1998).

[40] A. SCHILLER and K. INGERSENT, Physical Review B **51**, 4676 (1995).

[41] M. FABRIZIO and A. O. GOGOLIN, Physical Review B **51**, 17827 (1995).

[42] R. Egger and A. Komnik, Physical Review B **57**, 10620 (1998).

[43] S. Fujimoto and S. Eggert, Physical Review Letters **92**, 037206 (2004).

[44] L. Langer, V. Bayot, E. Grivei, J.-P. Issi, J. P. Heremans, C. H. Olk, L. Stockman, C. Van Haesendonck, and Y. Bruynseraede, Phys. Rev. Lett. **76**, 479 (1996).

[45] A. Bachtold, C. Strunk, J.-P. Salvetat, J.-M. Bonard, L. Forro, T. Nussbaumer, and C. Schonenberger, Nature **397**, 673 (1999), ISSN 0028-0836, URL http://dx.doi.org/10.1038/17755.

[46] A. Fujiwara, K. Tomiyama, H. Suematsu, M. Yumura, and K. Uchida, Phys. Rev. B **60**, 13492 (1999).

[47] P. L. McEuen, M. Bockrath, D. H. Cobden, Y.-G. Yoon, and S. G. Louie, Phys. Rev. Lett. **83**, 5098 (1999).

[48] S. Frank, P. Poncharal, Z. L. Wang, and W. A. Heer, Science **280**, 1744 (1998), http://www.sciencemag.org/cgi/reprint/280/5370/1744.pdf, URL http://www.sciencemag.org/cgi/content/abstract/280/5370/1744.

[49] M. Bockrath, D. H. Cobden, J. Lu, A. G. Rinzler, R. E. Smalley, T. Balents, and P. L. McEuen, Nature **397**, 598 (1999).

[50] J. Nygard, D. H. Cobden, and P. E. Lindelof, Nature **408**, 342 (2000).

[51] B. Babic, T. Kontos, and C. Schonenberger, Physical Review B **70**, 235419 (2004).

[52] T. W. Odom, J. L. Huang, C. L. Cheung, and C. M. Lieber, Science **290**, 1549 (2000).

[53] Explicitly, for the right movers the only non-vanishing commutation relations read $[\rho_{r=+1,\sigma}(-q), \rho_{r=+1,\sigma}(q)] = \sum_k (n_{k-q} - n_k)$. By invoking the last of the stated Luttinger liquid assumptions, we find that $\sum_k (n_{k-q} - n_k) = \sum_{k>k_0} (n_{k-q} - n_k) = \sum_{k_0-q\le k\le k_0} n_k = Lq/2\pi$. Here, k_0 is a high momentum cut-o which is taken to infinity at the end of the calculation. Similar relations are found for the left movers ($r = -1$). Taken together, we find the operators $\rho_{r,\sigma}(q)$ to be unnormalized Bose operators: $[\rho_{r,\sigma}(q), \rho_{r',\sigma'}] = \delta_{\sigma,\sigma'}\delta_{r,r'}\delta_{q+q',0}(rqL/2\pi)$

[54] The Klein factors connect states differing by one electron. When the thermodynamic limit is taken in a gapless system, there is, for all practical purposes (the computation of correlation functions), no differences between states containing N and $N1$ particles. However, when gaps open up, giving rise to finite correlation lengths, caution must be exercised when dealing with these operators. The literature contains several examples of calculations which were later discovered to be incorrect, precisely due to this subtlety.